EFFECT OF THERMOMECHANICAL PROCESSING ON THE PRECIPITATION BEHAVIOR OF A COBALT BASE SUPERALLOY : SUPERCO-605

by

KESHAB CHANDRA PATRO

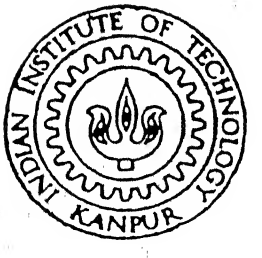

DEPARTMENT OF MATERIALS AND METALLURGICAL ENGINEERING

INDIAN INSTITUTE OF TECHNOLOGY KANPUR

FEBRUARY, 1998

EFFECT OF THERMOMECHANICAL PROCESSING ON THE PRECIPITATION BEHAVIOR OF A COBALT BASE SUPERALLOY : SUPERCO-605

A Thesis Submitted
in partial fulfillment of the requirements
for the degree of
MASTER OF TECHNOLOGY

by
KESHAB CHANDRA PATRO

To the
DEPARTMENT OF MATERIALS AND METALLURGICAL ENGINEERING
INDIAN INSTITUTE OF TECHNOLOGY KANPUR
FEBRUARY , 1998

MME-1998-M-PAT-LFF

Entered the System

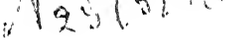

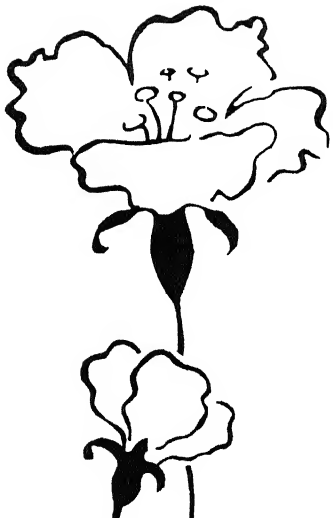

dedicated
to
my parents

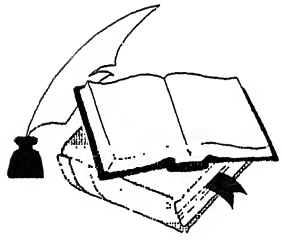

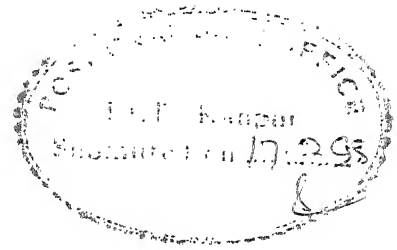

CERTIFICATE

This is to certify that the work in this thesis entitled "**Effect of thermomechanical processing on the precipitation behavior of a cobalt base superalloy: Superco-605.**" has been carried by Mr.Keshab Chandra Patro under our supervision and that it has not been submitted elsewhere for a degree.

(Dr.Sanjeev Bhargava)
professor

(Dr. Sandeep Sangal)
Associate Professor

Department of Materials and Metallurgical Engineering
Indian Institute of Technology, Kanpur -208016

ACKNOWLEDGMENTS

I wish to express my gratitude and indebtedness to my supervisors Dr. Sanjeev Bhargava and Dr. Sandeep Sangal for their inspiration, encouragement and guidance throughout my thesis work. Their constant advises made this work very interesting .

I would like to acknowledge the help , I got from Mr. Satyam Suwas through out the work. I would also like to thank Mr. K. P. Mukharjee and Mr. B. K. Jain for their helps at various stages .

I owe my thanks to my friends Sailesh , Raju , Arun , Babu , ... for their helps.

Keshab Chandra Patro

(Keshab chandra patro)

Contents

Chapter 3

Chapter 4

LIST OF TABLES

LIST OF FIGURES

ABSTRACT

The effect of thermo-mechanical processing on the grain boundary reaction as well as on matrix precipitation in the interior of the grains were investigated using a Wrought Cobalt base superalloy Superco-605 with composition Co-20Cr-10Ni.15W.0.08c-1.5 Mn. The alloy was solution annealed at 1250°C for 1h and 30 min., then 65% of deformation was given through hot rolling at four different temperatures (850°C, 950°C, 1050°C and 1150°C). The aging characteristics of solutionized as well as hot rolled samples were investigated using optical and scanning electron microscope (SEM). SEM revealed a greater continuity of precipitates along the grain boundary in the undeformed samples Vs. deformed samples. The extent of matrix precipitation that occurred during aging was also influenced by thermo-mechanical treatment. The activation energy of precipitation formation reaction was estimated as 207 kJ/Mole for the early stage of the grain boundary precipitation reaction in undeformed samples, and was considered to be the activation energy of grain boundary diffusion of chromium.

The activation energy of precipitation reaction for the samples deformed at 850°C and 1150°C was also estimated as approximatly 50 kJ/Mole which is around one fourth of the activation energy that obtained for undefformed samples. This low activation energy is attributed to the stress assisted diffusion of chromium through dislocation pipes. Rockwell hardness of all deformed samples were measured after aging and was produced a systematic decrease in hardness with increasing aging temperature. But no systematic relationship was observed between the hardness and the working temperature of thermo-mechanically processed sample. After aging, the hardness of solutionized samples was observed below 8 Rc which was well below the hardness of thermo-mechanically processed samples (20 - 50 Rc).

CHAPTER 1

INTRODUCTION

1.1 COBALT BASE SUPERALLOYS :- A GENERAL SURVEY

The search for high strength, high temperature materials has been continuous throughout the history of material science. For example, the demand for enhanced efficiency and performance of jet engine demands for high gas turbine combustion temperature, which has necessitated the development of materials that would have high creep and fatigue resistance at the same temperature. Figure 1.1[1], shows the materials properties demanded by the major components of a gas turbine engine. All these properties cannot be achieved in a single metal superalloys development responds to the need for materials with all these properties mentioned in Figure 1.1. At the same time superalloys gives a very good resistance to surface attack at high temperature. Modern high performance air craft jet engine could not operate without the major advances made in superalloys development over past 50 years.

The base elements of superalloys are cobalt, nickel or iron. These are group VIIIA elements. Several factor standout. For instance, the characteristic FCC structure is close packed. This is best atom arrangement to provide strength to very high fraction of the melting point (Co become FCC at high temperatures). The low thermal expansion coefficients to close tolerances to achieve maximum efficiency., High thermal conductivity helps in the cooling of turbine hot stage parts. Some primary physical properties of these base elements are given in Table 1.1.

Table. 1.1. Some physical properties of superalloy base elements

Element	crystal structure	Melting point (in °C)	Density (in g/cm^3)	Expansion Coefficien (in°C X10^{-6})	Thermal Conductivity (in cal/cm^2/s/ °C/cm)
Co	HCP	1493	8.9	12.4	0.215
Ni	FCC	1452	8.9	13.3	0.165
Fe	BCC	1535	7.87	11.7	0.175

Among these superalloys cobalt base superalloys has several advantages over Ni- and Fe-base superalloys. Some of the major advantages are given below [1]:

- Cobalt alloys exhibit higher melting temperatures and correspondingly flatter stress rupture curves, providing useful stress capability to a higher absolute temperature then Nickel- or Iron-base alloys.
- Cobalt alloys offers superior hot corrosion resistance to the contaminated gas turbine atmosphere due to their higher chromium contents.
- In general, cobalt alloys exhibits superior thermal fatigue resistance and weldability to nickel alloys.
- Capability to be melted in air and argon, in contrast to vacuum melting required for nickel-base and iron-base superalloys containing the reactive materials Aluminum and titanium.
- Incipient melting temperature of Nickel-base and Cobalt-base superalloys are very similar.

Due to these primary reasons cobalt base superalloys are unavoidable materials in gas turbine engine. The components which demands cobalt and chromium as a major alloying elements are shown in Figure 1.2, [2].

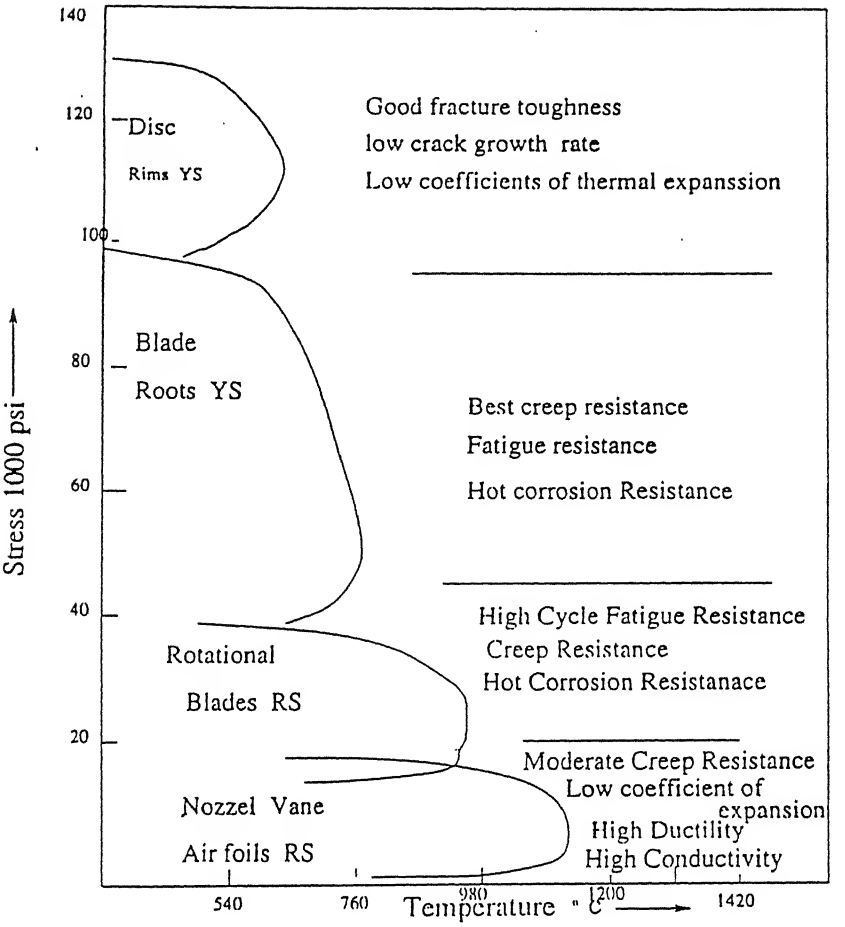

Fig.1.1 Gas Turbine engines major components and their material properties.

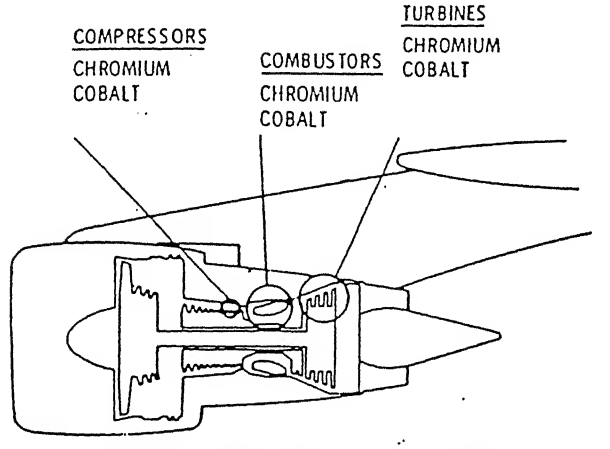

Fig 1.2 Current gas turbine engines depend on cobalt for several major components.

1.2 APPLICATIONS OF SUPERALLOYS

Although superalloys have a wide range of application and outstanding potential. The majority of today's superalloys are used in aircraft gas turbine industry. An approximate distribution of superalloys used in various applications in United States are given in Table 1.2,[3].

Table. 1.2. Distribution of superalloys application in the various fields

Aerospace:	
• Gas turbine	72%
• Air frame	8%
Power generation:	
• Gas turbine	10%
• Nuclear	2%
• Fossil	1%
Chemical:	6%
Miscellaneous:	1%

The bulk tonnage is used in gas turbine engine. Some of the end user applications categorized below [4].

- **Aircraft Gas Turbine:** Disks, Combustion Chambers, Bolts, Casing, Shafts, Exhaust Systems, Blades, Vanes and Burner Cans.
- **Stream Turbines Power Plant:** Bolts, Blades, Stack gas reheaters.
- **Reciprocating Engine:** Turbocharger hot plugs, Exhaust Valves.
- **Metal Processing**: Hot work tools and dies, Casting dies.
- **Medical Applications:** Dentistry uses, Prosthetic devices.
- **Space Vehicles:** Aerodynamically heated skins, Rockets Engine Parts.

- **Heat Treating Equipments:** Trays, Fixtures, Conveyer Belts, Baskets, Fans and Furnace Mufflers.
- **Nuclear Power Systems:** Control rod drives, Valve Stems, Springs, Ducting.
- **Coal Gasification and Liquification Systems:** Heat exchanger, reheater, Pipings.

Application of various wrought and cast Co-base Superalloys can be grouped according to use:

- High Temperature Application Materials: At temperature range 650°C, 1150°C includes S-816, Hayens 25, Hayens 188, Hayens 556, and UMCo-50.
- Fastner Alloys: For use about 650°C, includes MP35N and MP159.
- Wear-Resistant Materials: Stellite 6B.

Hayens 25 is perhaps best known wrought Co-base alloy and has been widely used for hot section of gas turbines, Nuclear reactors, devices for surgical implants and in cold worked condition, for fastners and wear pads. Hayens 188 is an alloy that was specially designed for sheet metal components, such as combuster and transition ducts, in gas turbines. The wear resistance material Stellite 6B is characterized by high hot hardness and relatively good resistance to oxidation. Where as its hot hardness properties is obtained through the formation of complex carbides of the Cr_7Co_3 and $M_{23}C_6$ types. Stellite 6B is widely used for erosion shields in steam turbines, for wear pads in gas turbines.

1.3 SUPERCO-605 - A COBALT-BASE SUPERALLOY

Superco605 is a cobalt base superalloy manufactured by MIDHANI, Hyderabad, India. Its composition is Co-20Cr-10Ni-15W-3Fe-1.5Mn-0.08C-0.3 (max. others). It is a quite similar composition to L-605. So its properties are also more or less similar to that of L-605 and HS-25. Some physical properties of these materials are given in Table 1.3 [5].

Table 1.3 Physical properties of cobalt base superalloy-wrought and cast

Specific gravity	8.2–9
Density	8200–9000 kg/m^3
Solidus/liquidus	14.7 W/m °C
Coefficient of linear expansion (20–100 °C)	9.5–11 × 10^{-6}/ °C
Electrical conductivity	1–2% IACS (copper 100%)
Specific resistance	850–17000 microhm mm
Young's modulus of elasticity	179–248 × 10^9 N/m^2
Impact	Will vary considerably
Fatigue strength (10^6 cycles)	± 250 N/mm^2 (applies to Stellite X40)

Hot strength

	Temperature in °C														
	20			650			760			870			980		
	UTS MPa	YS MPa	El %	UTS MPa	YS MPa	El %	UTS MPa	YS MPa	El %	UTS MPa	YS MPa	El %	UTS MPa	YS MPa	El %
I. Wrought alloys															
HA 188	960	485	56	740	305	70	710	305	61	635	290	43	420	260	73
L 605	1005	460	64	800	250	59	710	240	35	455	260	12	325	240	35
II. Cast alloys															
HS 21	680	–	2	500	–	3	470	–	5	380	–	16	220	–	35
X 40	745	525	9	515	260	12	485	–	10	325	–	16	200	–	31

UTS = ultimate tensile strength; YS = yield stress; El = elongation.

The stress (in MPa) for rupture in 1000 h of cobalt base superalloys at different temperatures.

	Temperature in °C			
	815	870	980	1095
I. Wrought alloys				
HA 188	110	70	25	–
L 605	117	72	26	–
II. Cast alloys				
HS 21	98	91	48	–
X 40	138	103	55	–

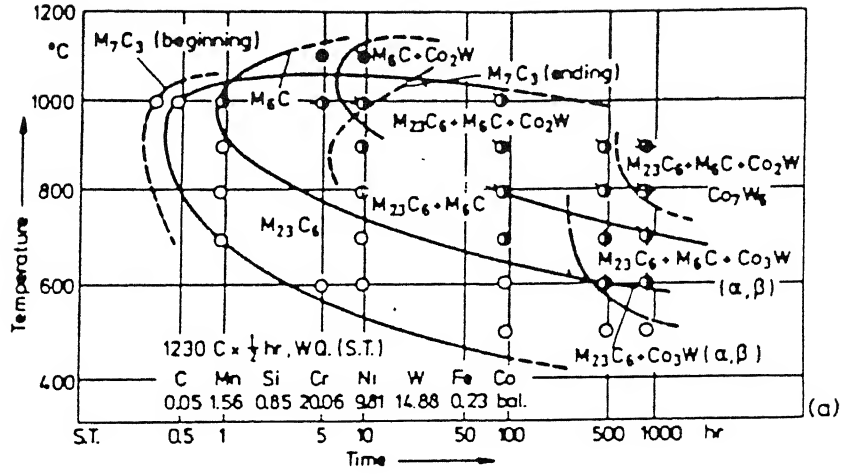

FIG. 1.3 TTT diagrams for a Co-base alloy L-605 (0·01 % C–20 % Cr–10 % Ni–15 % W–1·5 Mn bal.Co).[22]

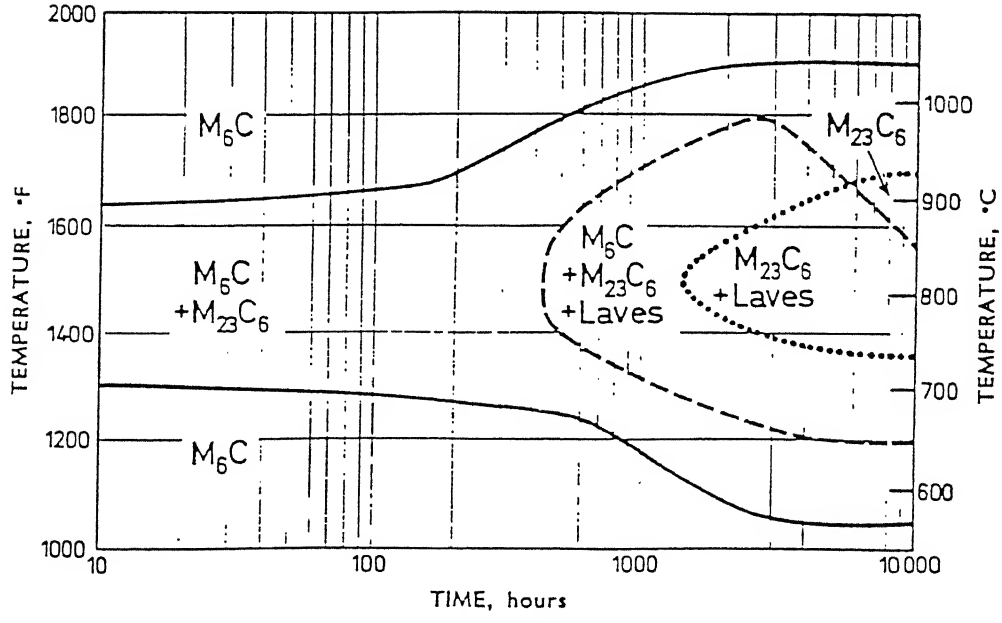

Fig. 1.4 Time-temperature-precipitation diagram on aging Haynes 188
Nominal composition: Co - 20-24% Cr - 20-24% Ni - 13-16% W
0.15% C - 0.03-0.15% La - 0.20-0.50% Si - up to 3% Fe - up to 1.25% Mn

Superco-605 is based on solid solution of cobalt, chromium and tungsten. It has additions of nickel to improve the ductility, while carbon and carbide formers are added to increase the hardness. It has the ability to retain its hardness at elevated temperatures and this with its corrosion resistance is the principal reason for its existence. This is not a complete solid-solution alloy because it contains secondary phases in the form of carbides ($M_{23}C_6$, M_6C, etc.) or intermetallic compounds. Aging causes additional second phase precipitation, which generally results in some loss of room temperature ductility. Among the chromium rich carbides, $M_{23}C_6$ is more favourable to form then M_7C_3 and M_3C_2 with this much of chromium carbon ratio present in the alloy. TTT diagrams of L-605[6] and H-188[7] (Fig. 1.3 and 1.4) shows that σ and Laves phases are also forms after a long time service exposure. These phases are deteriorated phases.

The size distribution, morphology, and extent of these phases are important in determining the effect on mechanical properties. The influence of heat treatment on properties is closely connected with microstructural features. The optimum combination of properties cannot be achieved in a single alloy. Compromise must be achieved by the alloy composition and the thermo-mechanical treatment.

1.4 OBJECTIVE OF THE PRESENT WORK

Although the behaviour of superalloys at elevated temperature attracted many researcher/engineers, there are lawless questions about the long term strength and stability of the microstructure. The importance of creep rupture ductility should be emphasized in long term service at high temperature. The stability of the microstructure in long term service exposure at high temperature is a strong function of the initial microstructure of the component.

Using heat treatment or thermo-mechanical processing techniques one can achieve the desired microstructure which would give the good creep rupture property for the alloy. As for as microstructure control is concerned, it is worth to know the effect of heat

treatment and thermo-mechanical treatment on precipitation behaviour of the alloy. The effects of solution treatment [8] and aging treatment [9,10] have been investigated for cast HS21 and HS188. No effort has been taken yet to study the effect of thermo- mechanical processing on precipitation behaviour of Superco-605.

So, in the present work, we have planned to study the effect of thermo-mechanical processing on the precipitation behaviour of Superco-605 alloy.

CHAPTER 2
LITERATURE REVIEW

2.1 CHEMICAL COMPOSITION OF COBALT BASE SUPERALLOYS

The chemical constitution of cobalt alloy is analogous to the general family of stainless steels, and the role of major and minor alloying elements is virtually identical throughout these austentic alloy systems. A list of alloying elements and their functions on microstructure is given [11] in Table 2.1

Table 2.1 Effect of several alloying elements in Cobalt base-superalloys.

Element	wt%	Effects
Cr	20-30	Oxidation and hot corrosion resistance; forms M_7C_3 and $M_{23}C_6$.
Mo; W	0-11	Solid solution strengthening; forms M_6C carbide; forms intermetallic compounds Co_3M.
Ta; Cb	0-4, Ta 0-9, Cb	Solid solution strengthening; forms MC and M_6C carbides; forms intermetallic compounds Co_3M.
A_l	0-4.5	Oxidation resistance; forms intermetallic compounds Co_2M.
T_i	0-4	Forms MC carbides; forms intermetallic compound Co_3T_i and with sufficient Ni, Ni_3Ti.
N_i	0-22	Stabilizes FCC matrix; forms intermetallic Ni_3Ti; facilitates working.
B; Zr	0.015-0.1, B	Improves rupture life through increased ductility; forms borides.
C	0.1-1.0	Forms carbides MC, M_7C_3, M_6C and $M_{23}C_6$.

Specifically, the key element chromium is added to impart hot corrosion resistance and oxidation resistance and some measure of solid solution strengthening where carbide

precipitation strengthening is a desirable feature, chromium plays a strong role through the formation of a series of varying chromium-carbon ratio carbides. A schematic phase diagram of Co-Cr-C ternary system is shown in Figure 2.1, [1].

Carbon is clearly critical to those casting alloys formulated for highest creep rupture strength levels, since carbide strengthening is primary precipitation hardening mechanism utilized in cobalt alloy systems.

The refractory elements tungsten and molybdenum are utilized as the major solid solution strengtheners for both wrought cast cobalt alloys. Of those alloying elements listed in Table 2.1. Only tungsten produces a favourable increase in melting temperature.

To enhance the stability of the high temperature face centered cubic cobalt matrix. additions of upto 20 wt% nickel or iron are used to suppress the transformation to hexagonal close packed cobalt at low temperature. These elements increases the stacking fault energy in cobalt alloy systems. The other elements which stabilizes of destabilizes the F.C.C. structure through the stacking fault energy interaction are shown in Fig. 2.2. [1]. The presence of these elements in wrought alloys lowers deformation resistance benefits workability. Additions are generally limited to 10 wt% in the cast alloys. since higher levels decreases rupture strength columbium, zirconium, and hafnium are generally more effective in a carbide forming role.

Aluminum has been added both wrought and cast cobalt alloys, as represented by sheet alloy S-57 and cast alloy AR-213, respectively. Additions of 5 wt% aluminum in each of these systems are high beneficial for oxidation and hot corrosion resistance. These alloys strengthened by uniform non-coherent precipitate of CoAl that generates properties similar to the carbide strengthened alloys CoAl tends to overage above approximately 760^{0}C.

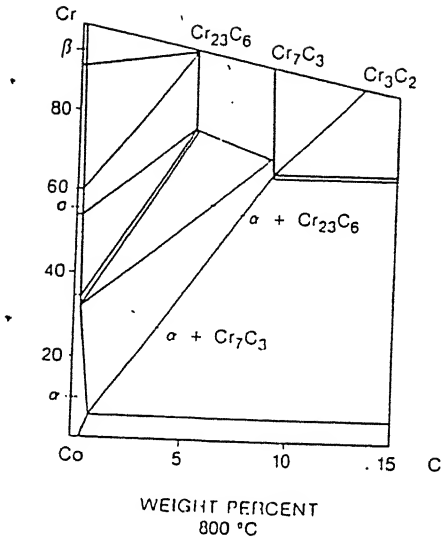

Fig.2.1 Schematic Co-Cr-C ternary phase diagram.

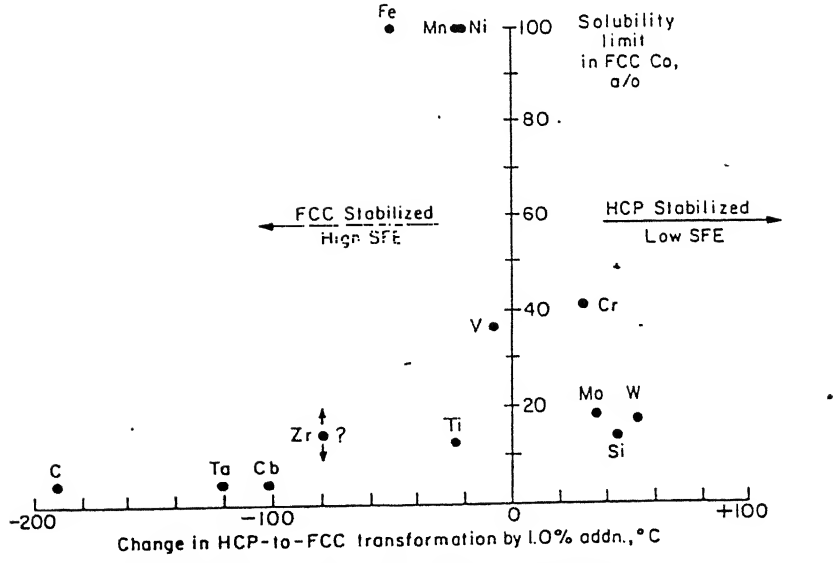

Fig.2.2 Effect of alloying additions on the HCP → FCC transformation in cobalt as a function of solubility in FCC cobalt.

In some cobalt alloys titanium is used to generate a uniform coherent precipitates of ordered FCC (Co, $Ni)_3Ti$ analogous to gamma prime in nickel alloys. However, titanium level above 5 wt% produce phase instability that produce the HCP-Co_3Ti or Co_2Ti Laves phases.

Boron is added to cast cobalt alloys to enhance rupture strength and ductility, however, its precise function in the microstructure is usually observed by the carbides. Addition of boron upto 0.1 wt% have been employed to provide additional strengthening.

2.2 MICROSTRUCTURES OF CO-BASE SUPERALLOYS

The rather complex composition of the alloys is designed to yield a critically balanced 'initial' structure consisting of several phase which may occur and their characteristic microstructural features are described below.

- **Matrix :**

The continuous matrix is a cobalt base austentic phase, usually contains a high percentage of solid solution elements such as chromium, tungsten, molybdenum, and nickel. Pure cobalt exhibits an allotropic phase transformation from the high temperature games FCC austentic crystal structure to the low temperature ε HCP structure at 417°C. Under equilibrium conditions, the addition of alloying elements will alter the thermodynamic stability of HCP and FCC polymorphs by either enlarging or constricting these fields.

- **Dispersion of Carbides :**

Contemporary cobalt alloys are strengthened primarily by precipitation of cubic, noncoherent carbide particles. These carbides are basically of two types, one is chromium rich carbides such as $M_{23}C_6$, M_7C_3 and M_3C_2. The other one is refractory element rich carbides such as MC and M_6C.

MC type carbides are considered to be a major factors in the strengthening of contemporary cobalt alloys, especially when properly balanced with $M_{23}C_6$. The strongest MC forming elements are, as indicated earlier, hafnium zirconium, tantalum, columbium, and titanium. In casting alloys the MC carbides generally precipitates as discrete bulky particles with regular features, such as diamonds and cubes. These are heterogeneously distributed over the matrix both intergranular, transgranular and interdendritic position. MC along grain boundary decreases the ductility. MC carbides does not breakdown easily during processing or solution treatment in the range of 1200 C to 1260 C. But MC carbides can, under long service exposures, degenerate to a lower carbides. Therefore, an important secondary hardening effect results from the MC carbide, which acts as a source of significant quantities of the $M_{23}C_6$ carbide[1].

M_6C type have complex cubic structure. It forms (if Mo or W is more than 6 wt% Cr content is less) during heat treatment of 815° C to 980° C. M_6C is generally exhibits excellent temperature stability, which is useful for grain size control during the fabrication of wrought materials. In some alloy it undergoes a transformation of M_6C into $M_{23}C_6$ following along term exposure reaction[4]:

$$M_6C + M' \rightarrow M_{23}C_6 + M''$$

M_6C may also forms as decompositional product of the MC carbides reaction with the alloy matrix[1]:

$$MC + \text{austentic} \rightarrow M_6C$$

that is,

$$TaC + (Co, Ni, Cr, C) \rightarrow (Co, Ni)_4(Cr, Ta)_2C$$

In some alloys acicular M_6C type carbides that forms in the matrix, degrades the rupture life and ductility. Aglomoration of bulky M_6C carbide leads to increase ductility but of lower strength[12].

$M_{23}C_6$ type carbides are forms in alloys with moderate to high chromium content. during low temperature heat treatment and service 760 °C to 980 °C from both degenerated MC carbides and from residual carbon in alloy matrix. These are usually forms at grain boundary, and occassionally along twin bands, stacking faults. These are discrete and irregular in shape. $M_{23}C_6$ can have also cellular structure due to improper heat treatment which leads to premature failure. In general, the lowest aging temperatures will produce the finest precipitates with the greatest increase in tensile strength[1]; conversely. ductility decreases. The coarser precipitates is more desirable for high temperature creep rupture strength and ductility[4]. A solution treatment can dissolves all the $M_{23}C_6$ carbides and increases the ductility but soften the matrix. Where along term aging can generates a significant quantity of reprecipitated fine $M_{23}C_6$ carbides that have markedly negative effect on low temperature ductility. Fig.2.3[1] , illustrates this behaviour for alloy MM509 exposed at 1500 F. So the initial microstructure of these alloys needs a balanced distribution of MC and $M_{23}C_6$ in order to compromise with the ductility of the component after a long term service exposure.

$M_{23}C_6$ carbides exert a profound influence on properties by their precipitation on grain boundaries Betteridge and Franklin [13] were the to identify the critical role of $M_{23}C_6$ carbides in Nickel base super alloys properties. A chain of discrete globular $M_{23}C_6$ carbides were found to optimize creep rupture life by preventing grain boundary sliding in creep rupture while concurrently providing sufficient ductility in the surrounding grain for stress relaxation to occur without premature failure.

In contrast, if carbide precipitate as a continuous grain boundary film. properties can be severely degraded. These effect were illustrated by Decker and Freeman in a study of the behaviour of Rene 80[1]. Figure.2.4. illustrates a well developed grain boundary in Rene 80 that has finally initiated fracture (cracking) during rupture testing. In these cases rupture failure can initiate either by fracture of these grain boundary $M_{23}C_6$ particle or by decohesion of $M_{23}C$ interface.

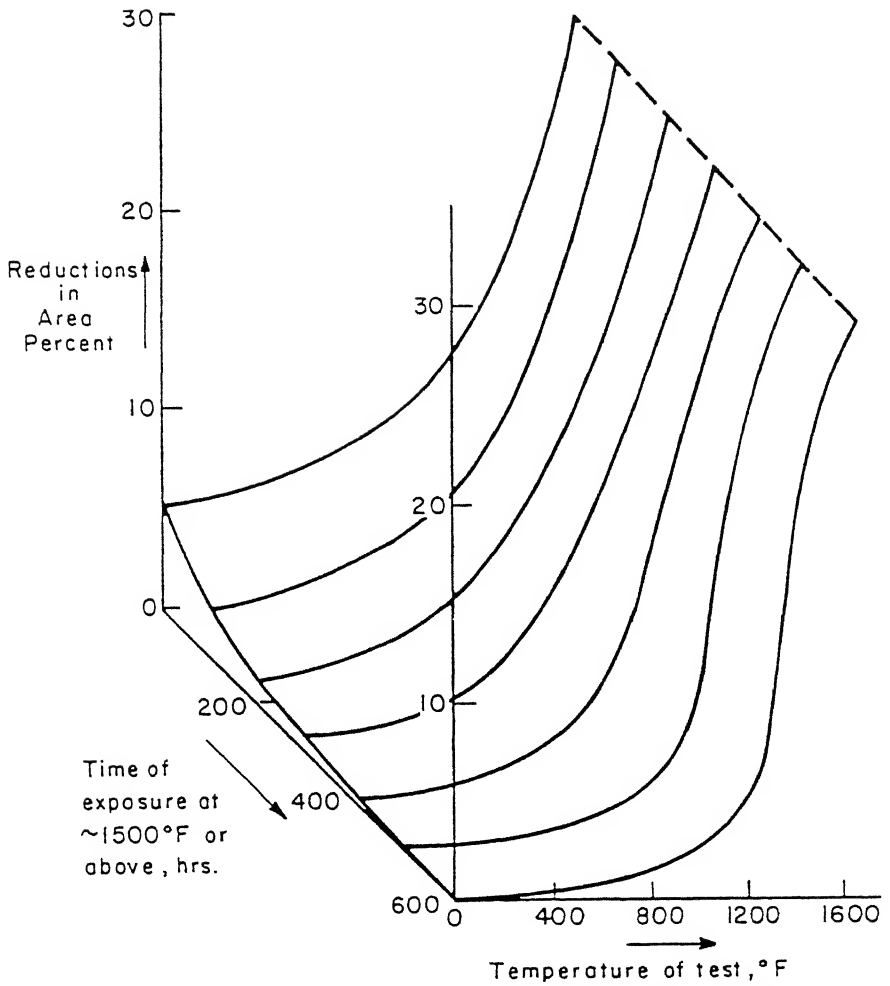

Fig.2.3 Effect of exposure at elevated temperatures on the residual ductility of cobalt superalloys. MM-509 used as a guide.

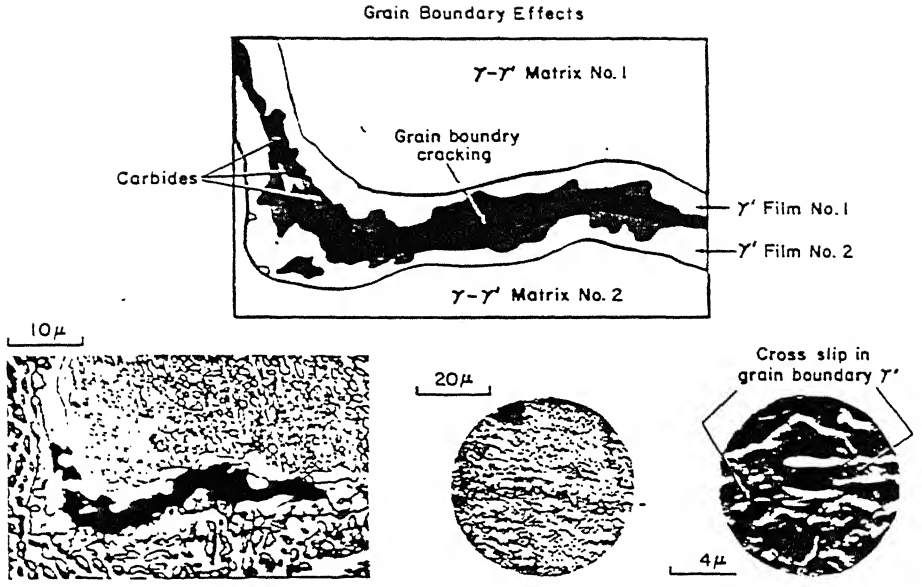

Fig.2.4 Flow and fracture behavior in the grain boundary of René 80.[61]

M_3C_2 and M_7C_3 are forms at low chromium carbon ratios. M_3C_2 is rhombic and it forms peritectic reaction with chromium; it has been found in some early superalloys M-C. M_7C_3 is trigonal in structure. It is metastable and the decomposition reaction from M_7C_3 to $M_{23}C_6$ generates potent secondary carbide strengthening according to the following reactions:

$$23Cr_7C_3 = 7Cr_{23}C_6 + 27C$$

$$6C + 23Cr = Cr_{23}C_6$$

- **GCP Phases :**

Geometrical close packed (GCP) phases have the form A_3B, where A is the smaller atom and the phase is an ordered phase, coherent precipitates with in the FCC austentic matrix, the generation of GCP phase within cobalt alloy is substantially more difficult since the chemical and crystallographic stability is effected by lattice mismatch that is rarely less than 1 wt%[1]. During late 1950s two commercial cobalt alloys were briefly popular. J-1507 and J-1650. These were strengthened by an ordered, coherent gamma prime precipitates stabilized by the high nickel content; hence, the GCP phase was actually $(Ni, Co)_3Ti$. The alloy identified CM-7, is carefully balanced to minimize the formation of η and laves phase in service[14]. While gamma prime phase is reportedly stable to 843^0C. high stresses will accelerate the transformation to η above about 802^0C.

- **TCP Phases**

Topological closed packed (TCP) phases that have been observed in cobalt alloys are σ, μ, and laves, π is related semicarbide phase also observed. Laves has been observed often in cobalt alloys; it is common in L-605, and found occasionally in S-816 and HS-188.

It is worth noting that these phases precipitates in both acicular and/or blocky morphologies in cobalt alloys. Conversely reduction strength may be associated with removal of the strengthening elements from the matrix. These are hard intermetallic compounds unfit as ductile alloy bases and not yet generally found useful as strengthening phases. In superalloys their formation is avoided. Interestingly, sigma is structurally closely related to the common $M_{23}C_6$ carbide. Considerable lattice coherency exits between sigma and $M_{23}C_6$, so that sigma often nucleates on $M_{23}C_6$[15]. The same reasoning can be applied to the μ phase. μ has a similar close structural relationship with the carbide M_6C. In alloys that develop M_6C, excessive concentrations of molybdenum and chromium can be expected to lead to formation of μ rather than σ, although the rule is not fast. The laves phases, with an A_2B formula, contains atoms bonded by 'size' factors; examples are Co_2Mo or Co_2Ta.

The composition of this Co-base superalloy is Co-20 Cr-10 Bu-15W 1.5 -0.08 C. In this composition Cr has higher tendency to form carbides.

Among the chromium rich carbides, M_7C_3 can form if the chromium to carbon ratio is below '3' for higher chromium-to-carbon ratio, $M_{23}C_6$ is most likely to form (Fig.2.5) [1]. Among the refractory element rich carbides, M_6C may form because of high tungsten content. MC carbides forms with trace elements in the alloy. Absence of elements like lTi and Al indicates there may not be any intermetallic phase present other than cobalt-tungsten system. M_6C is generally forms in alloy having low chromium content [1]. So below the solvus temperature of $M_{23}C_6$, $M_{23}C_6$ precipitation content may be high enough compared to M_6C, MC and Co_3W (if any). However, no attempt has been taken to identify the different precipitates. Fig.1.3 and Fig.1.4 the phase diagrams for L-605 and HS-188 also shows that, short term aging process does not produces any intermetallic and/or deteriorated TCP phases.

Due to size misfit chromium is energetically more stable at grain boundaries than in matrix. This causes a flux of chromium from interior of the grain to grain boundaries at elevated temperature. So the grain boundaries acts as nucleation sites for chromium

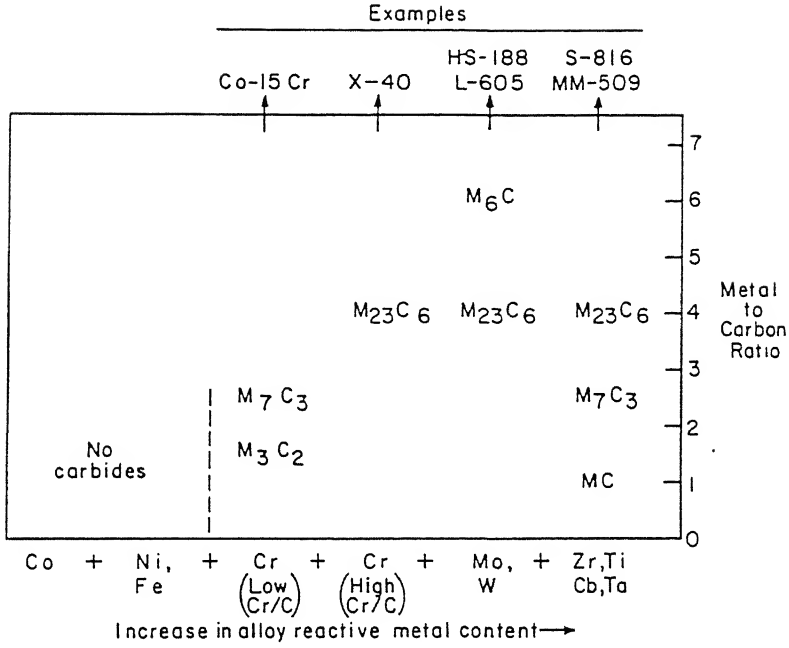

Fig.2.5 Effect of adding elements of varying electronegativity on type of carbides formed in cobalt superalloys, carbon assumed 0.1–0.6%.[12]

carbide through their enhanced diffusion rates and the ability to accomodate relatively large mismatch[16].

2.3 HEAT TREATMENT AND RUPTURE PROPERTIES

To achieve an optimal microstructure for a specific application the heat treatment should consist of

(I) a solution heat treatment stage; and

(ii) precipitation aging treatment stages.

An approximate TTT diagram will be helpful in understanding the influence of time and temperature on microstructure, although for extended aging times diagrams are available for few superalloys.

Effect of heat treatment on rupture behaviour of X-40 tested at 815^{0}C and 30 ksi is shown in Figure2.6[17]. This figure shows that the rupture life is minimum for cast material then the solutionized material. A solutionizing treatment followed by an aging treatment has gives still higher rupture life. Early heat treatment for wrought alloys such as M-502 and nimonic 80A consisted principally of only a high temperature solution treatment followed by a low temperature aging treatment. This generated good tensile and short time rupture properties but did not stabilize the structure sufficiently to produce optimized long time rupture properties. Heat treatments for these two alloys were studied by Heckman [1] to correct these failing. An additional intermediate temperature was added to each respective heat treatment to drive the MC degeneration equation forward. The results are shown in Figure.2.7 .

Figure.2.8 shows the effect of different aging temperature on generation of improved rupture strength by carbide precipitation in Vitallium[18]. $M_{23}C_6$ plays a dominant role at about 1400 F, probably as a result of degeneration of M_7C_3 and MC. At this temperature rupture strength becomes highest sacrificing its ductility. We there rupture ductility or strength of aged material is improved over that obtainable from solution treated materials depends generally on the test temperature, test time, and the particular alloy. Thus the figure.2.9 shows that rupture strength at 1200 and 1350 F was

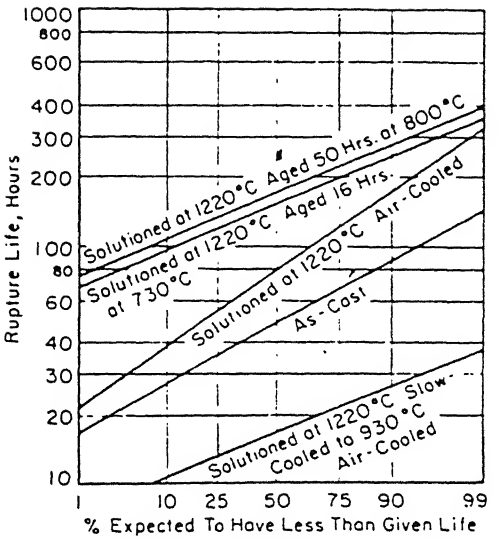

Fig.2.6 **Effect of heat treatment on rupture behavior of X-40 tested at 815 °C (1500 °F) and 207 MPa (30,000 psi).**

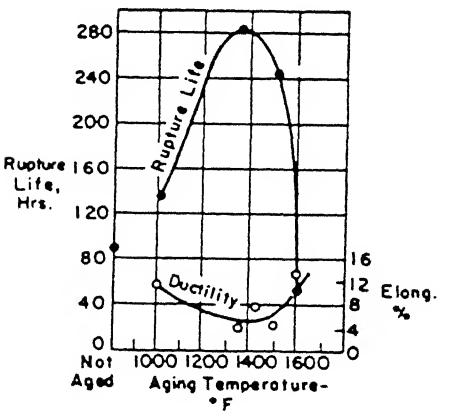

Fig.2.8 **Effect of aging on the rupture life and ductility of as-cast Vitallium at 1500 °F and 20,000 psi.**

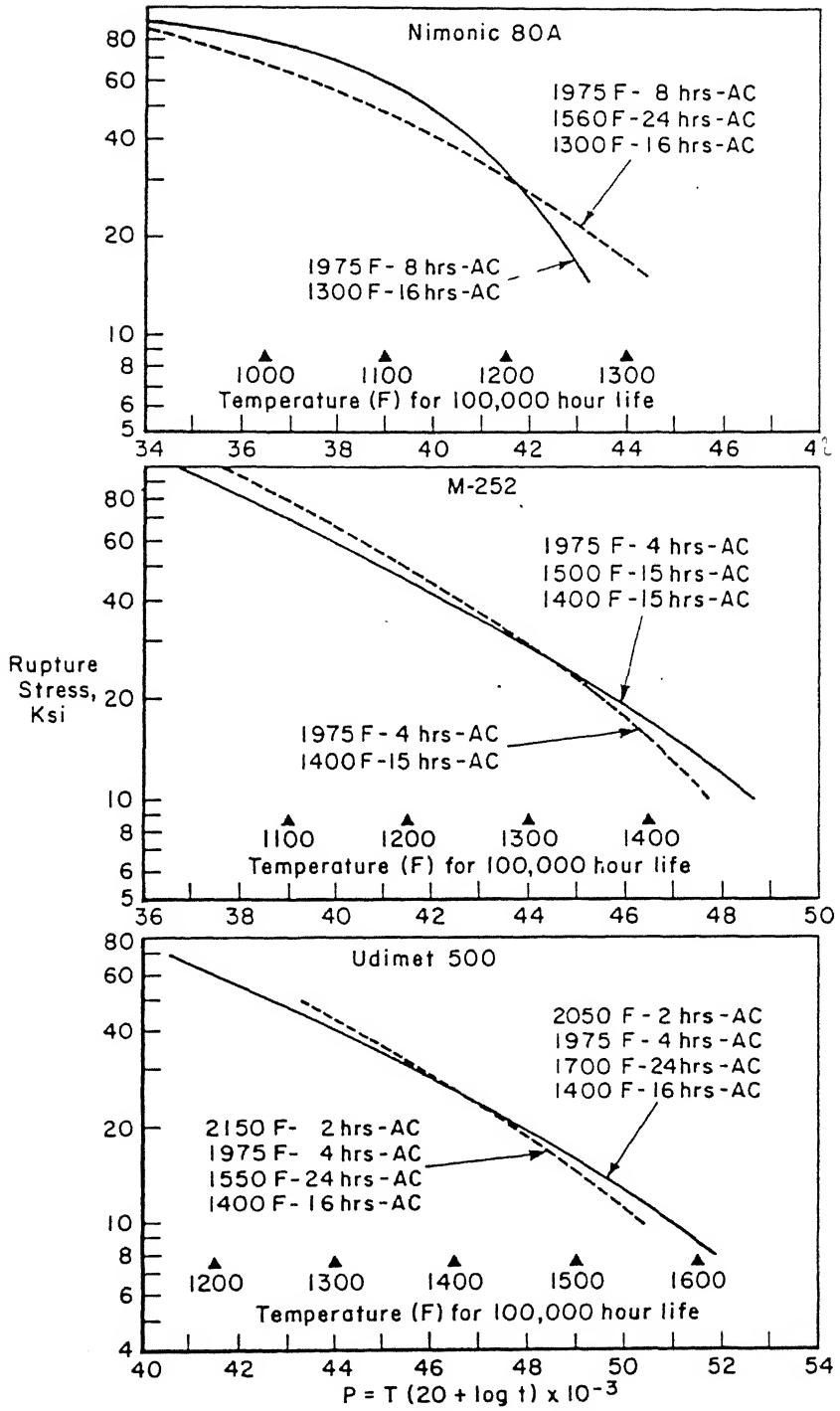

Fig.2.7 Effect of increasing intermediate aging on rupture properties of wrought superalloys

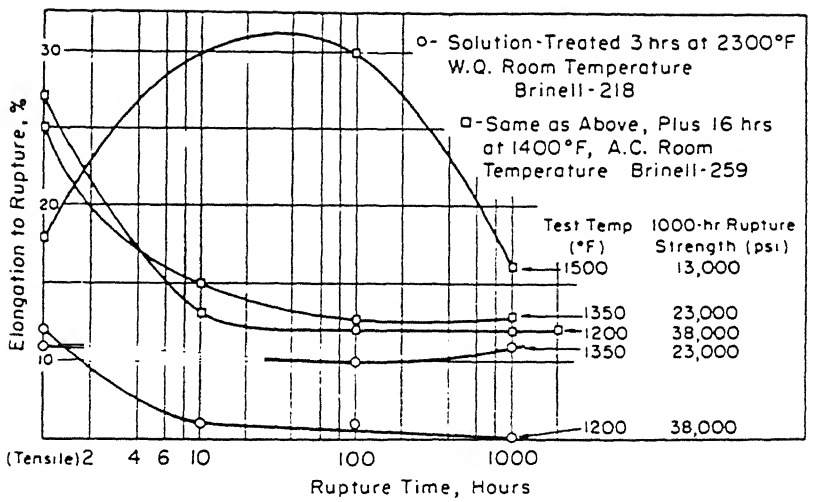

Fig.2.9 **Effect of aging on the elongation to rupture of S-590.**

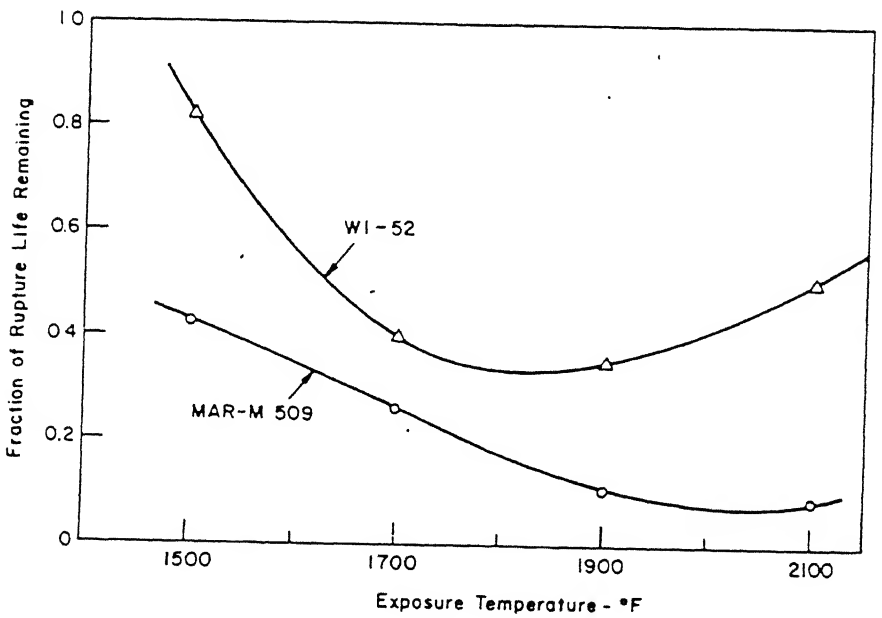

Fig.2.10 **Effect of 100-h prior exposure at various temperatures on the rupture lives at 1500 °F and 35,000 psi of WI-52 and MAR-M509 cobalt-base superalloys.**

not increased by aging at 1400 F, but that the elongation to rupture was improved in S-509[17].Creep rupture bars of WI-52 and MM509 were exposed at no load for 100h at temperature ranging from 1500 to 2100°F prior to a creep rupture test at 1500°F and 35 ksi.Fig. 2.10 shows that both alloys rapidly lost strength due to exposure to approximately 1900°F[17]. This loss was attributed to the combined effect of second phase agglomeration(overaging) and partially breakdown of carbides (MC in MM509 and M_6C in WI-52) and reprecipitation as acicular $M_{23}C_6$, a morphology that is less efficient for strengthening. At temperature above 1900°F, $M_{23}C_6$ precipitation is not favored, and the principal effect of high temperature exposure is then agglomeration and dissolution of the strengthening phases.

Klarstrom has demonstrated [1] that thermo-mechanical processing (TMP) of thin to 015 in] sheet can improve the low strain (<1%) creep strength of HS 188 by developing a strong recrystalized texture. TMP consisted of 80% final cold working followed by an anneal at 1232 C for 10 min.

2.4 MAJOR STRENGTHENING MECHANISMS IN CO-BASE SUPERALLOYS

The strength of commercial superalloys arises from a combination of hardening mechanisms, including contributions from solid-solution elements, particles and grain boundaries. In addition, thermo-mechanical processing is sometimes utilized to provide strengthening through increased dislocation density and the development of a dislocation substructure. In this section, we would like to discuss only few of these mechanisms, which could be applicable to our system Superco-605.

2.4.1 Solid Solution Strengthening

In a solid solution the solute atom effect on various physical or crystallographic properties, for example lattice parameter and elastic modulus. Fleischer has shown [19] that both solid solution hardening and precipitation hardening can be accounted for by

accounted for by internal strains generated by inserting either solute atoms or particles in an elastic matrix. Tungsten is the most dominating solute with a volumetric misfit of $|\delta|$ = 0.12 for SF20 [20]. Cr and Ni cause the average increase in cobalt lattice parameter.

Flow stress of the solid solution strengthened matrix, for a given pair of strain and temperature can be expressed as follows [21]:

$$\sigma_m = \sigma_{co} + \Sigma W_i C_i$$

where,

σ_m = flow stress of matrix

σ_{co} = flow stress of pure cobalt

C_i = Concentration of ith solute

W_i = Strengthening factor [unit, Mpa/at.%]

W_i increases with increasing melting temperature and yield strength of the constituents.

2.4.2 Composite Hardening

In the regime where the matrix deforms plastically and the carbide deforms elastically, the composite stress can be written as

$$\sigma_c = f_m \sigma_m + \Sigma f_{carbide} C_{carbide}$$

This relationship is used to explain the observed hardness in SF20 [22]. Table.2.2. shows the observed results.

2.4.3 Order Hardening

Order hardening by shearable precipitates could arise in the alloy if there is any ordered precipitates in the matrix.The maximum possible hardening by ordered

precipitates can obtained at a specific volume fraction only [22]. The shear stress involved in weak dislocation pair coupling is less than the shear stress involved in strong dislocation pair coupling in the shearing mechanisms.

4.4 Orowan Looping

For strong spherical obstacles generally, orowan looping dominate over the shearing mechanism. Because the stress needed for shearing the precipitates in larger compared with the stress needed to bypass these particles by an orowan looping mechanism. The smaller the precipitate size and higher the volume fraction, the larger will be the orowan hardening. Van otterloo et al [22] has observed it in SF20, that is shown in Table. 2.3

2.4.5 Work Hardening

The flow stress due to dislocation-dislocation interaction is also very high. Work hardening results through an increase in the dislocation/slip band density at low temperature of working. Viatour et. al. [14] shows the variation of hardness Vs. amount of deformation and aging temperature, for a Cobalt base alloy CM-7 is given in Table 2.4. Pugliese et.al[23] also shown that a sharp increase in hardness and strength of a cobalt alloy after cold work.

Table.2.2. Composite hardening in SF20: A comparision between experimental and calculated result

Constituent	Vol. %	Elastic Limit	Total Hardness Calculated	Observed Hardness
Co	52	1.9 GPa	10.1 GPa	11.3 GPa
Co_3W	8			
M_7C_3	35	5.9 GPa		
$M_{13}C_6$	5	3.3 GPa		

Table 2.3. Effect of particle size and volume fraction on hardness of SF20

Particles	Mean size	Vol. %	Contribution to Hardness
Co_3W	0.5 μm	8	29 MPa
Carbide	1 μm	40	78 MPa

Table. 2.4. Effect of cold work and subsequent heat treatment on hardness of 2-mm CM-7 sheet

Heat treat (TC-1h,A.C	Amount of deformation, %				
	0	5	10	15	20
Cold worked	242	287	331	366	385
950°C	282	304	328	339(R)	318
1000°C	263	287	287(R)	275	287
1050°C	252	261(R)	258	270	275
1100°C	242	242	242	252	263
1150°C	214	223	232	242	242
1200°C	206	218	226	223	214
1250°C	214	214	214	214	206

.(R): onset of recrystalization.

Interaction between intersecting slip bands impede the further motion of dislocations, increasing the internal stress. A similar relationship to Hall-petch relation was employed in the case of Nimonic 80A to explain the hardening behaviour where the distance between slip band intersections was envisioned as being equivalent to small grains. The band spacing was analogous to the grain diameter in the Hall-petch model, as follows:

$$\sigma = \sigma_o + Ki^{-1/2}$$

where,

σ = Maximum stress

I = slip band spacing, and

σ_o, K = Constants for a given material

This can be observed from Fig.2.11 for Nimonic 80 A [24] and waspaloy [25].

2.4.6 Dislocation and Grain Boundary Interaction

The grain boundaries and twin boundaries also act as an obstacle to the dislocation motion which leads to the well known Hall-petch relation:

$$\sigma_y = \sigma_I + kd^{-1/2}$$

where,

σ_y = yield strength of a polycrystalline material

σ_I = yield strength for a single crystal of same material

d = average grain diameter

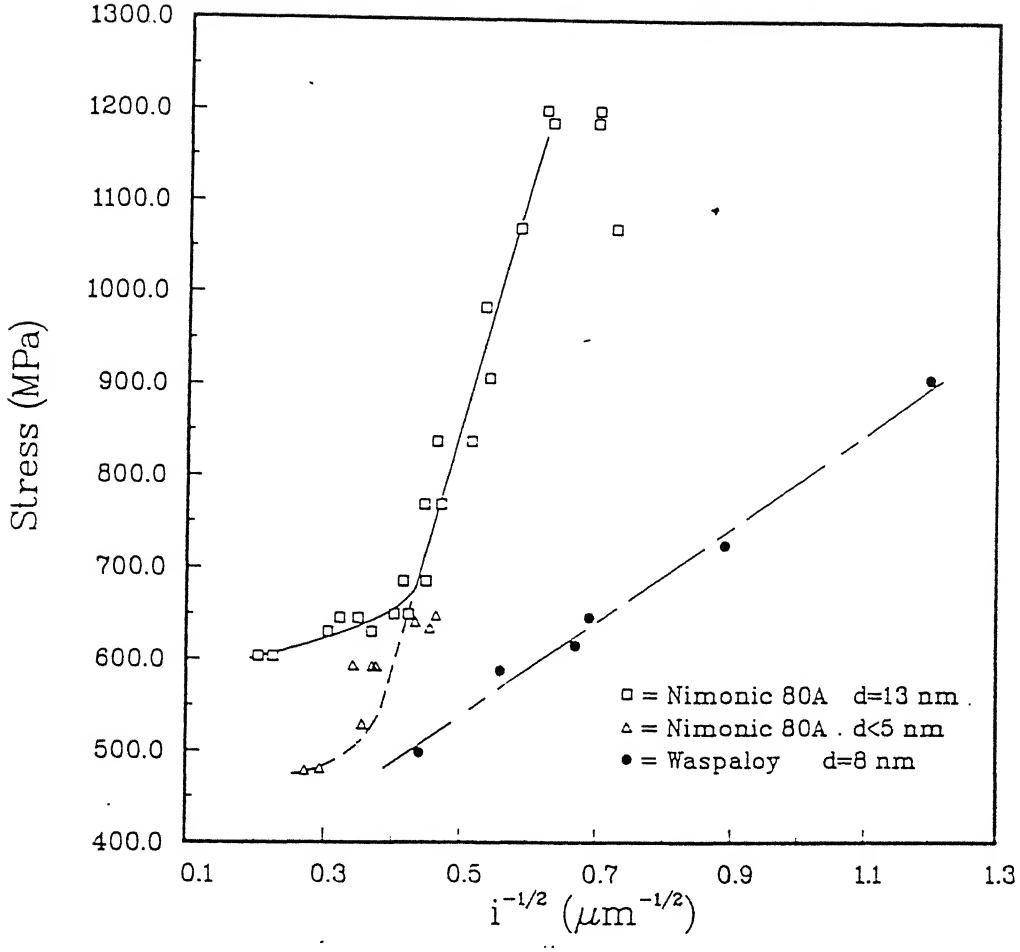

Fig.2.11 Stress response as a function of the slip band density for Nimonic 80A [32] and Waspaloy [22].

CHAPTER 3

EXPERIMENTAL PROCEDURE

In this chapter, the details of experimental techniques used during the present course of investigation are discussed in detail. Part A contains the details of starting materials used in the present work, part B deals with the description of equipments used and the experimental procedure involved during processing, whereas in part C, the details of various characterization techniques are discussed with all relevant information.

3.1 STARTING MATERIAL

The starting material used in the present investigation was supplied by Mishra Dhatu Nigam Limited, Hyderabad (India). The as received material was in the form of 32cmX9cmX0.6cm rectangular plate. The present alloy is a cobalt base superalloy Superco-605. Its chemical composition is given in Table 3.1.

Table 3.1: Chemical Composition of superco-605

Elements	Co	Cr	Ni	W	Mn	C	Fe
wt%	balance	20	10	15	1.5	0.08	3.0

The plate was cut into square pieces of 2.5 cm x 2.5 cm. These pieces used were used for thermomechanical processing.

3.2 THERMO-MECHANICAL PROCESSING

To study the effect of thermomechanical processing on the precipitation behaviour of Superco-605, specimens were processed in two routes. As shown in Fig. 3.1 , one is heat treatment process, which consist of a simple solutionizing treatment at 1250°C for 1 h and 30 min. followed by an aging treatment. The other route is thermomechanical

Fig.3.1. Material processing map

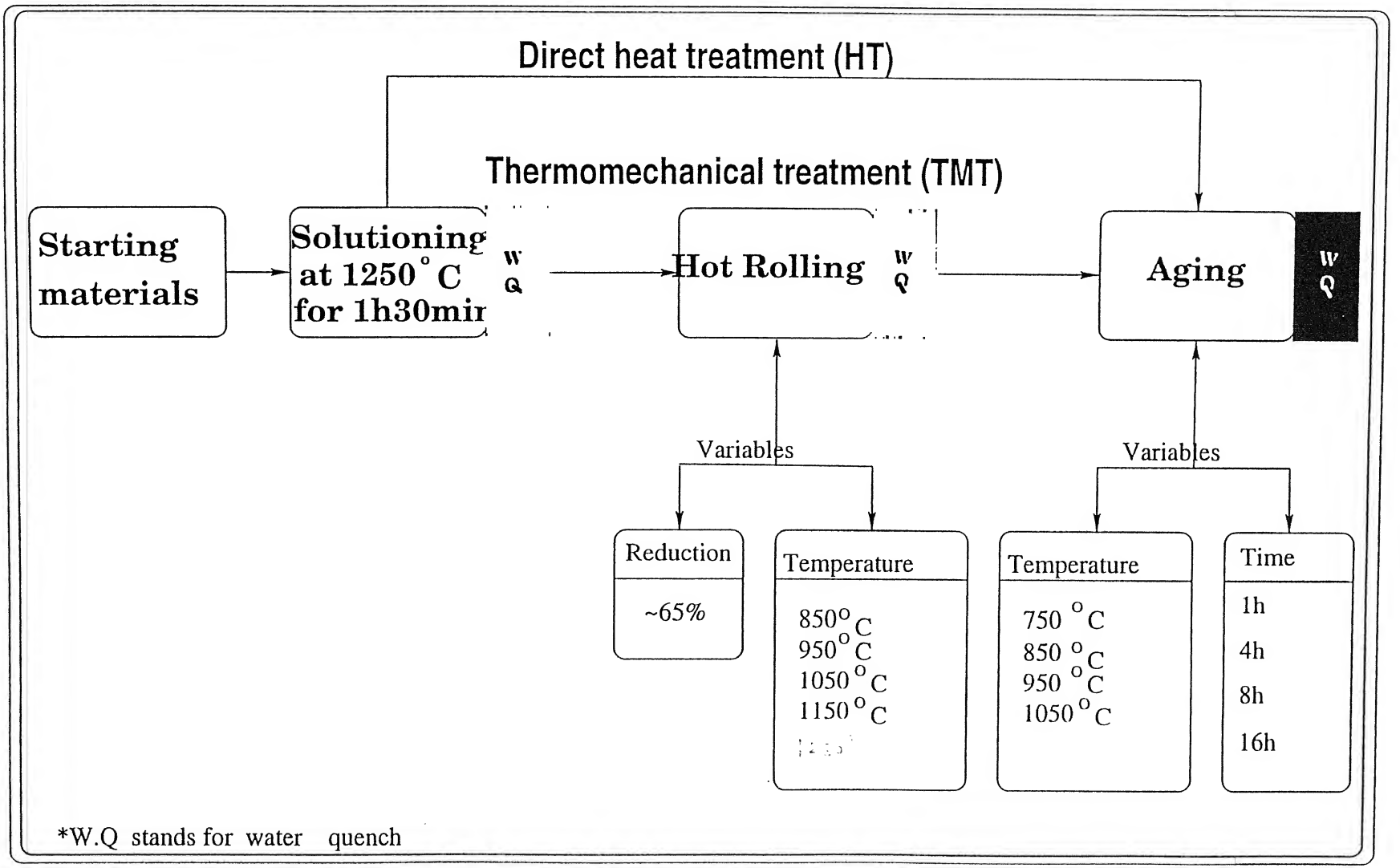

processing. It consist of a solutionizing, hot rolling and aging treatment in sequence are. A wide range of hot rolling temperature were chosen in between solutionizing temperature and much above the allotropic transition temperature of the alloy.

The design of the furnace was done such that it was capable of maintaining protective atmosphere. The furnace was having a constant temperature zone of 15 cm in length and was heated by silicon carbide rods. Muffle of the furnace consisted of an inconel tube, and was closed from one end. Gas was introduced in the furnace through a 4 mm internal diameter stainless tube passing through the closed end of the furnace. The furnace was mounted on wheels so as to bring it very close to the rolling mill.

Hot rolling was done on a 2 high rolling mill which had 135 mm diameter of the rolls. Speed of rotation for the hot rolling mill was kept at 55 rpm in all the experiments. No prior heating of rolls was done before hot rolling of specimen and they were maintained at room temperature.

Prior to the hot rolling, samples were soaked upto 25 minutes at the desired rolling temperature. After soaking samples were driven out and quickly fed to the feeding end of the rolling mill. After each pass the samples were fed back into the furnace for nearly 5 minutes so that it retains the rolling temperature. Again, it was pulled in the same manner and subjected to the second rolling pass. However, there was a very little drop in temperature till the time it could get rolled, which may be attributed to the quickness in the feeding process. The same sequence of operation was repeated till the samples acquired the final desired thickness. rolling was kept strictly unidirectional. The amount of per pass varied from 10% to 20%.

Solutionizing:

As given in processing map, figure 3.1, all the samples were solutionized at 1250°C for one and half hour, prior to hot rolling and/or aging. After solutionizing samples were water quenched. Fig. 3.2(a) and 3.2(b) shows the microstructures after

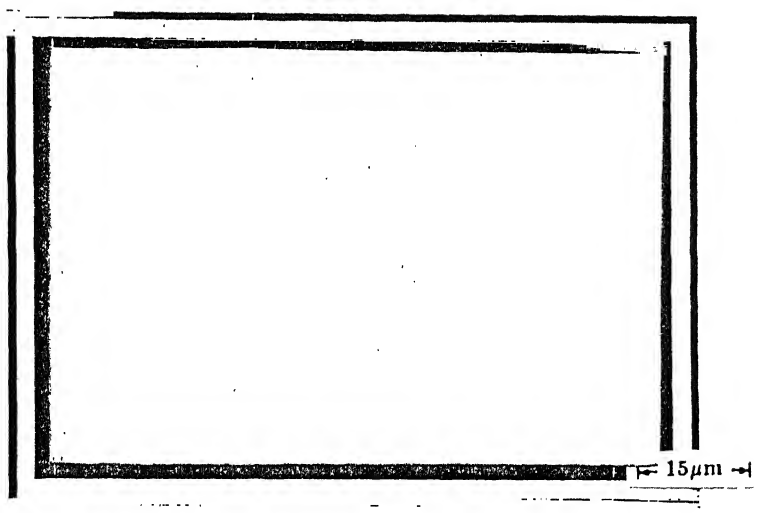

(a). Scanning electron micrograph

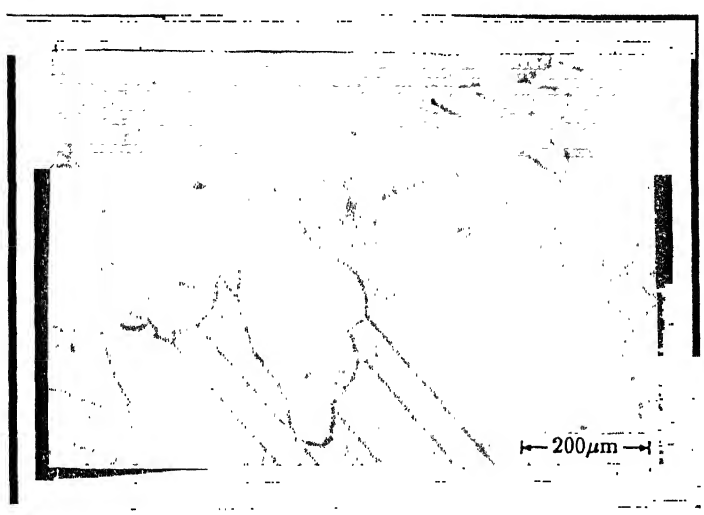

(b). Optical micrograph

Fig. . .SEM and optical micrograph of the samples solutionized at 1250°C for 1 hour and 30 min.

solutionizing treatment.These microstructure was showing no residual precipitate after solutionizing treatment.

Hot Rolling :

Hot rolling of solutionized samples were done for five different temperature. The hot rolling schedule are given in Table 3.2.This was a multipass rolling process. The rolling process is strictly followed as mentioned above. Samples were water quenched after final pass has given.

Table 3.2: Hot rolling schedule

Rolling Temp. (in °C)	Initial Thickness	Final Thickness (in mm)	% of Reduction
850		2.1	65.4
950		2.08	65.7
1050	6.07	2.36	61.1
1150		2.14	64.5
1250		2.64	56.5

Aging :

Aging was done in the same furnace. All samples were aged for different time and temperatures as mentioned in processing map Fig. 3.1. Since there four aging temperature and four different times, a total of 16 samples were made from each rolling condition. Samples rolled at 1250°C were aged only at 750°C and 850°C. All the samples were water quenched after aging treatment.

3.3 CHARACTERIZATION TECHNIQUES

The characterization techniques used in the present investigation can be classified under two headings: microstructural characterization and mechanical testing. The experimental details for all these are described below.

3.2.1 Microstructural Characterization

Microstructures of the as processed specimens were examined through optical and scanning electron microscopy. A few samples were examined under Leitz optical microscope. Prior to this, the samples were polished on emery papers (0 to 4 grades) followed by wheel polishing. With alumina powders of sizes 1 μm and 0.3 μm respectively. The polished samples were etched with an etchant of 92% HCl, 5% H_2SO_4 and 3% HNO_3. Microstructural observations were generally done on the longitudinal section of the specimen, along the rolling direction.

Most of the microstructural characterization in the present investigation were done with scanning electron microscope (JEOL-JSM 840A). The polished samples were seen under the scanning electron microscope operated at 15 kV using secondary electron radiation (SE mode).Quantitative metallographic techniques were used to calculate the grain size and volume fraction of precipitates. Volume fraction of precipitates were measured using a rectangular grid of 99 points. Fig. 3.3 shows the transparent grid used in the study. Since the number of grid points kept constant for all the measurements the relative error in the measurements were very. The aspect ratio of the grain were measured using lineal intercept method. The sample worked at 850°C and 950°C have intense shear bands. To make distinguish between grain boundary and shear band network. We have etched these sample with a mild chromic acid (02%). It etches only grain boundaries.

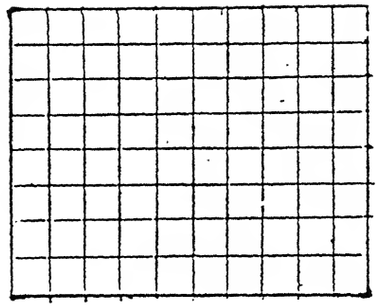

Fig. 3.3. Transperent grid used for matlographic measurement.

3.2.2 Mechanical Testing

In mechanical testing section, we have done hardness testing only. Hardness of all the samples were tried to measured in Rockwell 'C' scale using a 150 kg major load. Hardness of HT samples are below 10 Rc, so hardness of these sample were taken in Rockwell 'B' scale using 100kg load. Rockwell B is measured on a Rockwell hardness tester machine with 1/16 inch diamond ball.

CHAPTER 4

RESULTS AND DISCUSSION

As discussed in Chapter 2, the cobalt base superalloy, Superco-605, is a high-temperature alloy consisting of an austenite matrix and a variety of precipitated phases such as carbides and intermetallic compounds. The intermetallic compounds may, in turn, be of the type geometrically close-packed (GCP) and/or of the type topologically close-packed (TCP). The alloy superco-605 is strengthened primarily by the precipitation of cubic non-coherent carbide particles of the type M_6C and $M_{23}C_6$. However, it has also been observed that, depending on the composition and microstructural state the topologically close-packed laves phase may also precipitate in the alloy and may result into a poor low-temperature ductility of the alloy.

The precipitation behaviour of the carbide phases in cobalt base superalloys is known to be quite complex. However, little information exists in the open literature on the role of processing parameters in influencing the precipitation behaviour of carbides, in general, for cobalt-base superalloys. The conventional heat treatment of these alloys consists of a solution treatment at followed by an aging treatment.

Superco-605 alloy contains nickel, chromium and tungsten. Among these elements the addition of Ni is known to increase the stacking fault energy (SFE) of the alloy while those of Cr and W decrease the . . '' Therefore, it is expected that the alloy may undergo dynamic recrystallization during its hot deformation. The precipitation behaviour of carbides can therefore be considerably influenced by the hot rolling temperature depending on whether the dynamic recovery (DRV) or the dynamic recrystallization (DRX) occurs as the softening mechanism during hot rolling. The present chapter deals with the results in the precipitation behaviour of carbides as influenced by the hot rolling temperature. These results have been compared with those of obtained by the conventional heat treatment involving solution treatment and aging.

4.1 EFFECT OF SOLUTION TREATMENT ON THE PRECIPITATION BEHAVIOUR OF CARBIDES

Scanning Electron Microscopy revealed a greater continuity of carbides along the grain boundaries in simple heat treated (HT) samples. The continuity of precipitates along the grain boundaries increases with temperature up to 950°C. At aging temperature 1050°C the continuity of carbides along the grain boundaries was lower than that of observed at 950°C. Fig. 4.1(a) shows a dense near grain boundary carbides for aging temperature 850°C. These near grain boundary carbide were homogeneously distributed over the matrix, when the sample was treated at 950°C. This is shown in the fig. 4.1(b). But the matrix precipitation is totally absent in the samples aged at 1050°C, as shown in Fig. 4.1(c).

As far as good tensile and creep properties concerned these two microstructural characteristics: (I) continuity of carbides along grain boundaries and (ii) the lack of homogeneous matrix precipitation are undesirable.

The variation of grain sizes were also measured after aging treatment. The solutionized samples after aging treatment at various temperatures and times shows a narrow range of grain size variation. It indicates that no considerable grain growth occur in between 850°C to 1050°C temperature for 1 h to 16 h of aging. This is shown in Fig. 4.2. The grain sizes observed in this case were in the range of 500 μm to 600 μm.

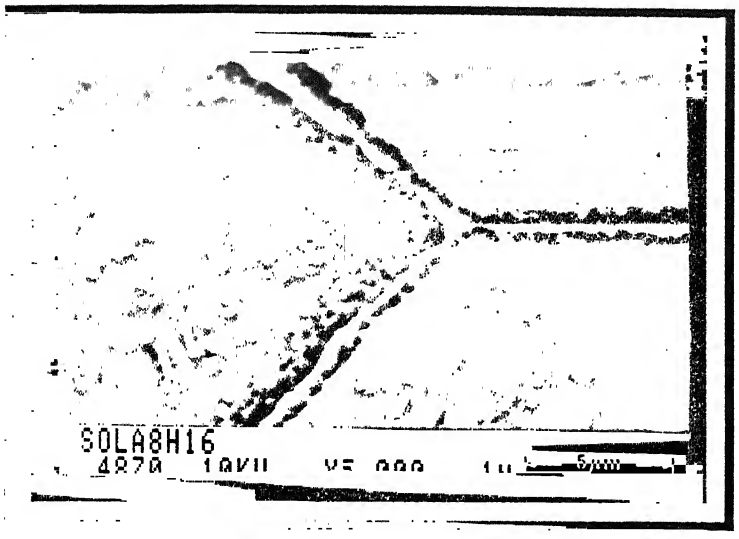

(a). Aged at 850 °C ,for 16h

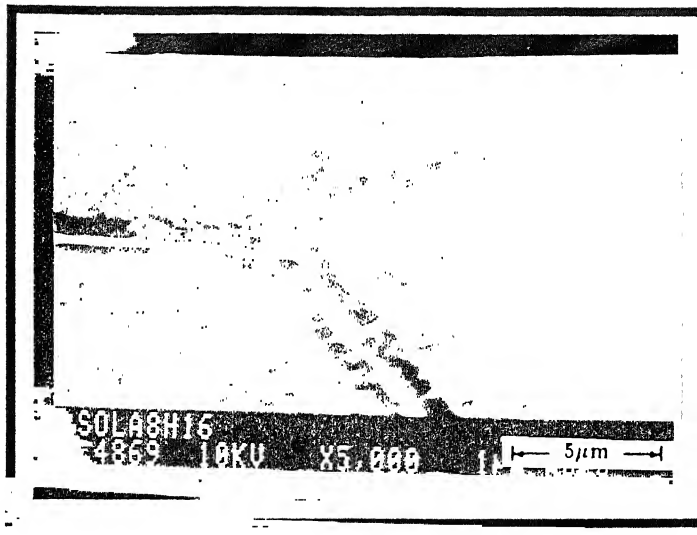

(b). Aged at 850 °C ,for 16h

(c). Aged at 950 °C ,for 16h

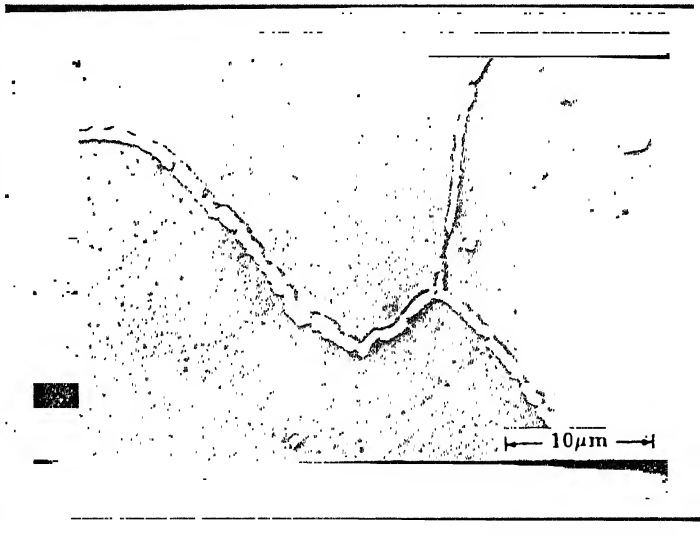

(d). Aged at 1050°C for 8h

Fig.4.1.Optical micrographs of the samples after solutionizing at 1250°C and aged at different temperature

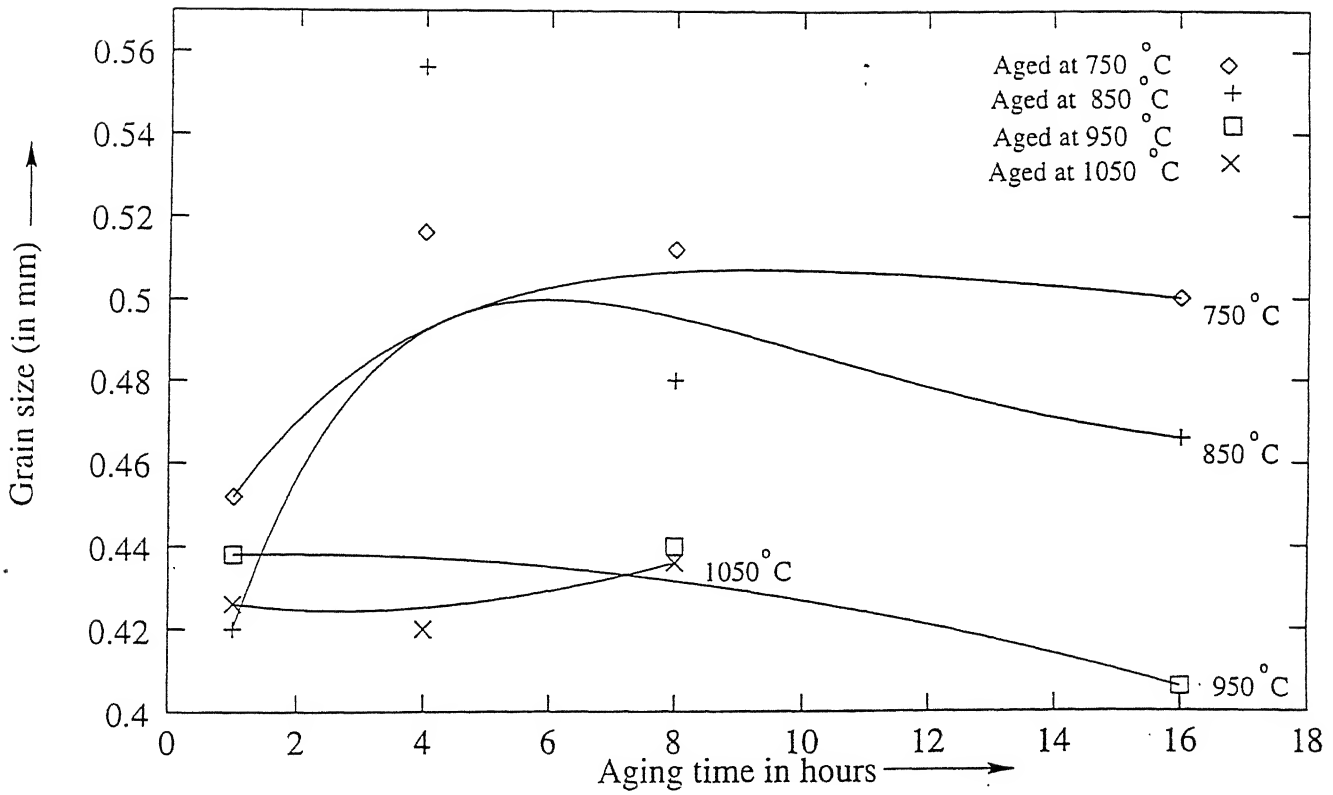

Fig.4.2 .Grain size vs aging time in solutionized sample after aging at different temperature.

4.2 EFFECT OF HOT ROLLING TEMPERATURE ON MICROSTRUCTURE AND HARDNESS OF AS ROLLED ALLOY

4.2.1 Effect of hot rolling temperature on the as rolled structure

After solutionizing samples of Superco-605 were hot rolled at different temperature as shown in Table 3.2. The amount of deformation was kept within 60% to 65%. Microstructures of hot rolled samples were analysed and the results are as follows:

Aspect ratios of grains were measured for all the samples. Aspect ratio increases with rolling temperature, till dynamic recrystalization temperature reach. Fig. 4.3 shows the variation of aspect ratio with rolling temperature. Aspect ratio of grain for rolling temperature 850°C was 13.4, and at 1050°C Rolling temperature it was 20. Aspect ratio drops to 1 ~ 2 at temperature 1150°C, it shows that dynamic recrystallization occurs at this temperature. Scanning electron microscopy revealed that the subgrain boundary formation starts during rolling at 1050°C. The aspect ratio of these subgrains are comes around 3.5. This indicates that partially recrystalization occurs at rolling temperature 1050°C.

Fig. 4.4 shows the microstructures of the samples rolled at 850°C and 950°C have intensive shear bands as well as highly elongated grain structures, where as the samples rolled at 1050°C shows only elongated grains and partially recrystalized grain structure. It did not show any shear bendings. In the microstructures of the samples rolled above 1050°C, as shown in Fig. 4.4(e) and 4.4(f) have neither any shear band nor elongated attain structure was observed. These microstructures are completely dynamically recrystalized. This result is also supported by hardness measurement.

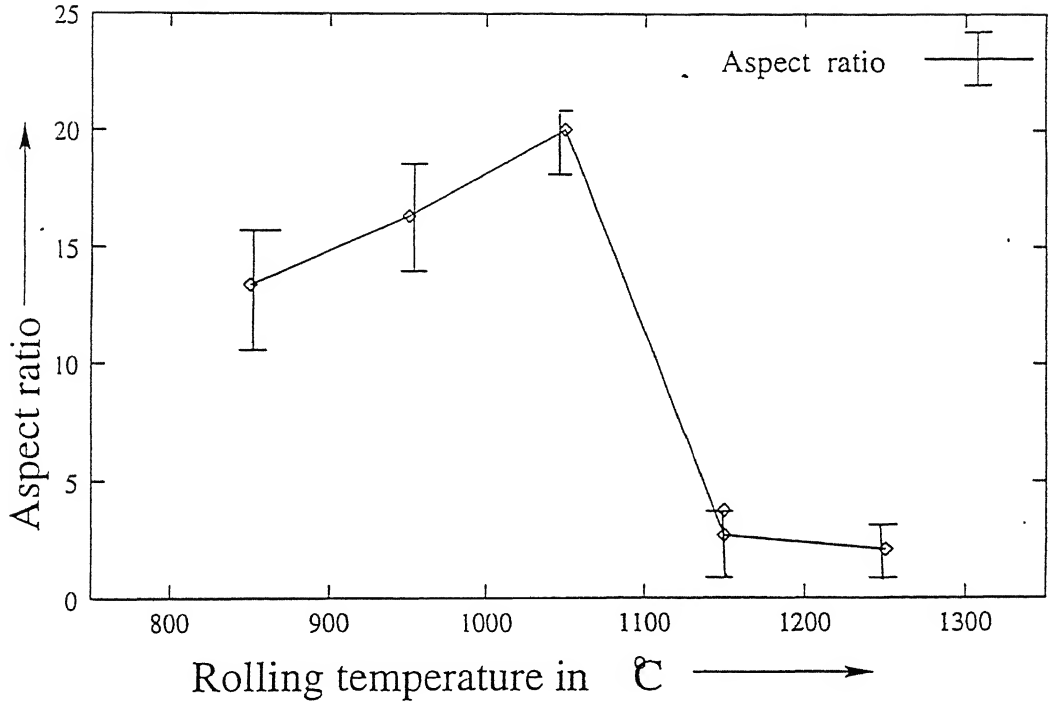

Fig.4.3 .Aspect ratio of the grains vs rolling temperature in the hot rolled samples.

#. The range of hardness observed for a particular condition is shown by the marker $\overline{\mathrm{I}}$.

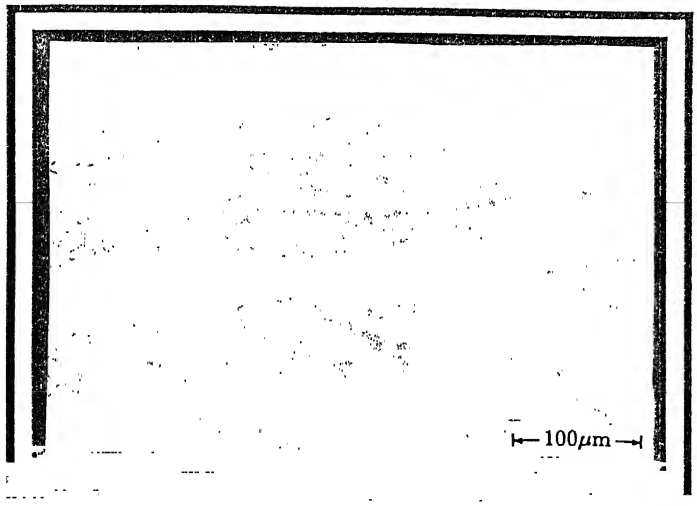

(a). Rolled at 850 °C

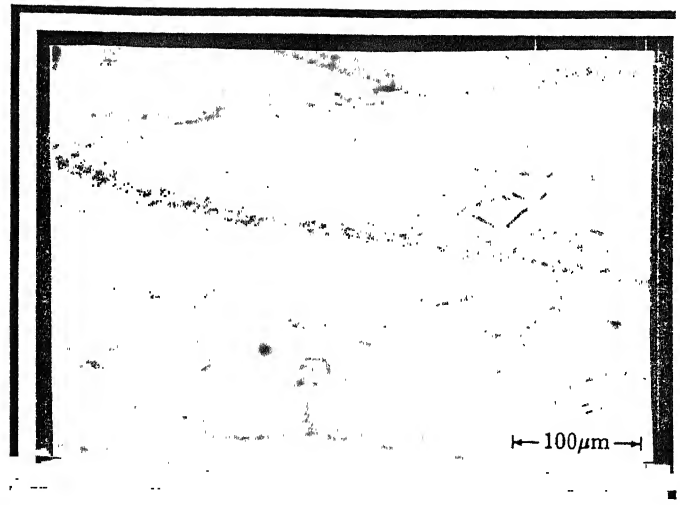

(d). Rolled at 1050 °C

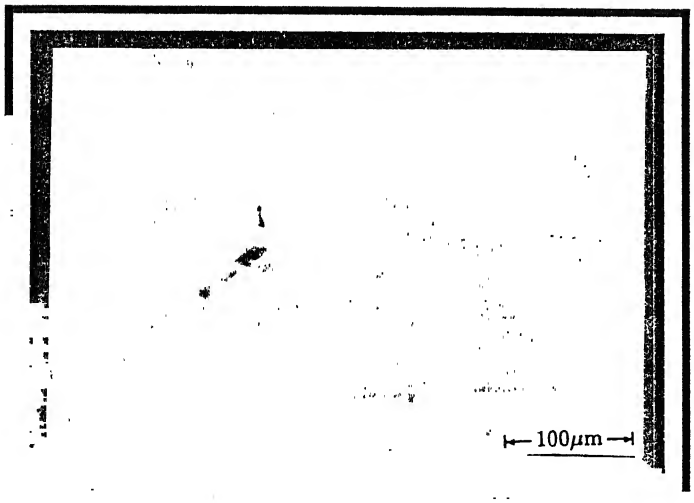

(b).(Rolled at 950 °C

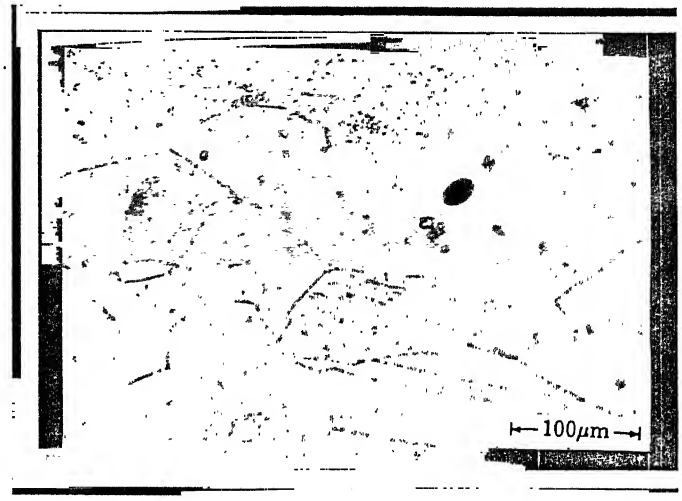

(e).Rolled at 1150 °C

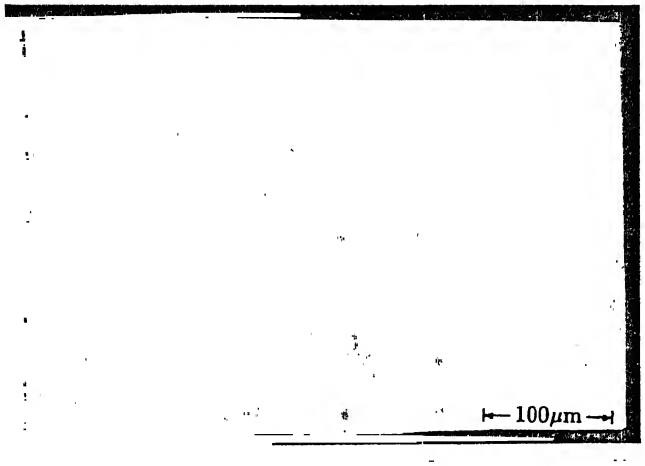

(c).Rolled at 1050 °C

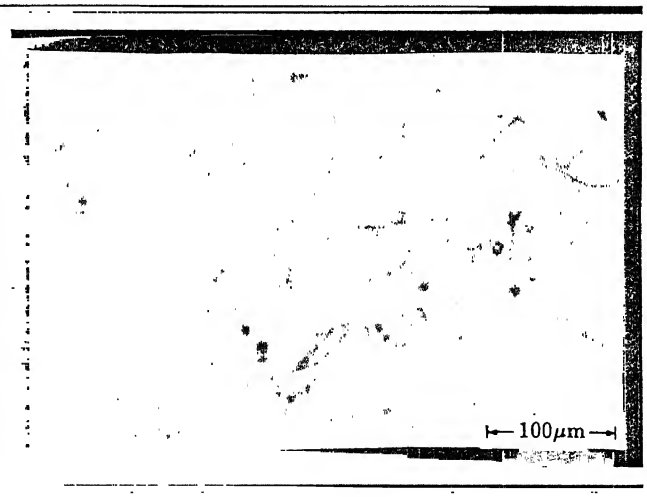

(f).Rolled at 1250 °C

Fig.4.4 .Optical micrographs of hot rolled samples

The grain sizes after hot working also measured. The grain size measured along rolling direction for samples worked below 1050°C are in the range of 1 ~ 1.3 mm for working temperature 1150°C and 1250°C grain sizes observed are around 75 μm ~ 90 μm.

4.2.2 Effect of Hot rolling Temperature on the Hardness of as Rolled Alloy

Hardness of the worked samples decreases with increase in working temperature. This is because of competition between recovery and work hardening processes. Recovery is the mechanism through which a material becomes softer and regains its ability to undergo additional deformation. For higher working temperature recovery process is more activated, and so hardness is decreases. Fig. 4.5 shows that there is a large drop in hardness for working temperature above 1050°C. It indicates both recovery and recrystallization processes were activated simultaneously at this temperature. This fact is supported by optical microscopic examination as shown in Fig. 4.4(a) to 4.4(f).

4.3 EFFECT OF HOT ROLLING TEMPERATURE ON MICROSTRUCTURAL EVOLUTION AND PRECIPITATION BEHAVIOUR OF CARBIDES

4.3.1 Recrystallization of the Structures

The samples rolled at 850°C gets recrystallized during aging at 950°C, gets recrystallized during aging at 1050°C. But the samples rolled at 1050°C gets recrystallize during aging at 750°C. This temperature is low enough compared to the recrystallization temperature needed for samples rolled at 850°C and 950°C. This is because the samples rolled at 1050°C were partially recrystallized during hot rolling. Table 4.1 shows that, the different samples gets recrystallized during aging at different temperatures.

The grain sizes in thermo-mechanically treated samples after recrystallization are low enough compared to directly heat treated samples measured grain sizes for some of

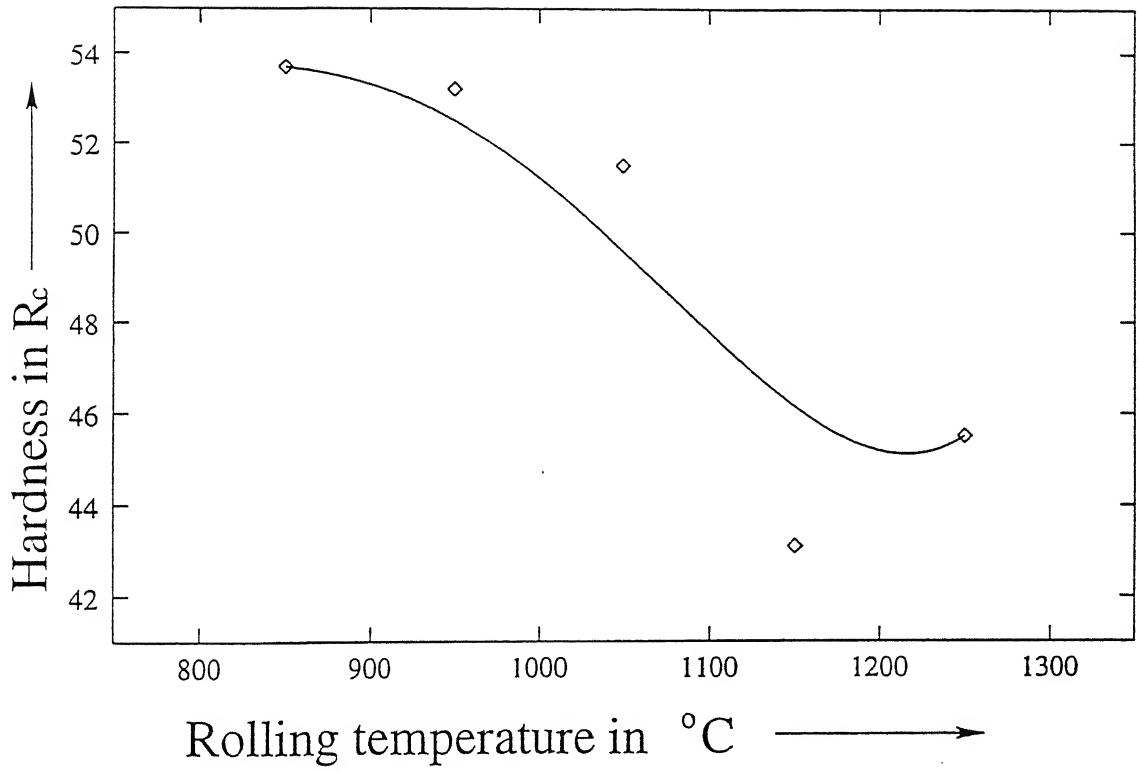

Fig.4.5 Hard ness vs rolling temperature in the hot rolled samples.

the samples is given in Table 4.2. The grain sizes were below 30 μm at aging temperature 1050°C, for samples rolled at 850°C and 1050°C. The microstructures of all the samples aged at 750°C and aged at 1050°C is shown in Fig. 4.6 and Fig. 4.7. The grain size distribution is quite in homogeneous in samples rolled at 850°C then the samples rolled at1050°C followed by an aging treatment at 1050°C gives largely inhomogeneous grain size distribution.

Table.4.1: Recrystallization during aging in TMT Samples.

Rolling Temperature (°C)	Recrystallization Observed during Aging Temperature (°C)
850	950
950	1050
1050	750
1150	Dynamically Recrystallized during Rolling
1250	Dynamically Recrystallized during Rolling

Table.4.2: Grain sizes after recrystallization in TMT sample

Rolling Temp. (°C)	Aging Temp. (°C)	Grain size (in μm) for aging times			
		1h	4h	8h	16h
850	1050	7.29	6.03	41.5	29.1
1050	1050	11.4	7.5	10.5	23.1
	750	12.3	7.5	11.4	25.8
1150	750	72	70.8	85.2	93.1
	850	47.4	82.4	91.5	64.4

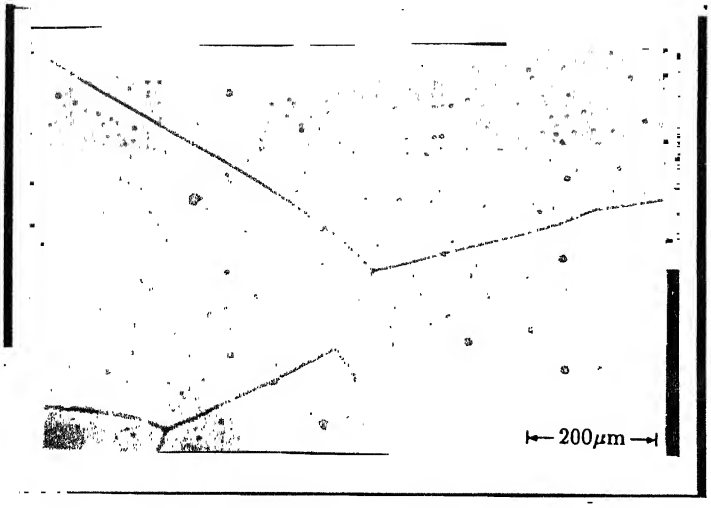

(a). Solutionized sample

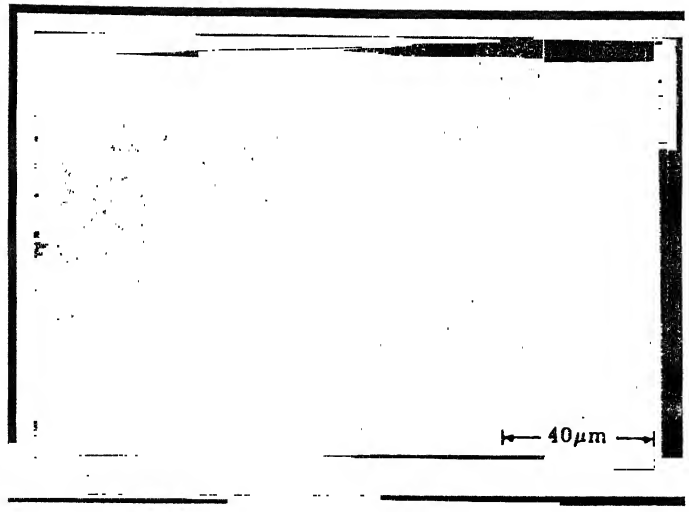

(d). Rolled at 1050 °C

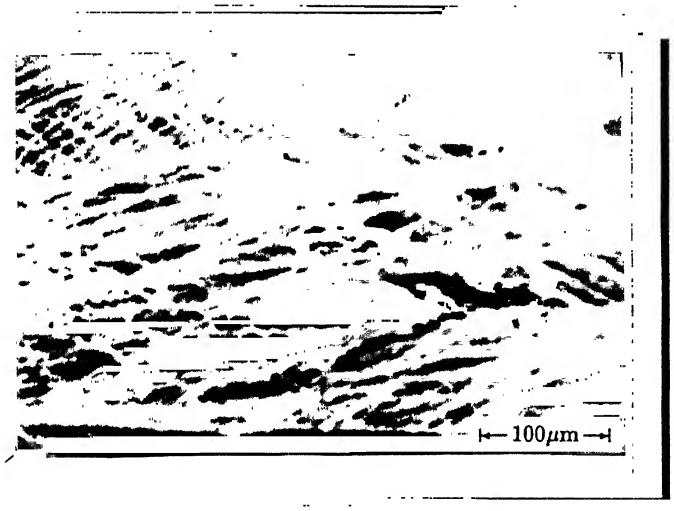

(b). Rolled at 850 °C

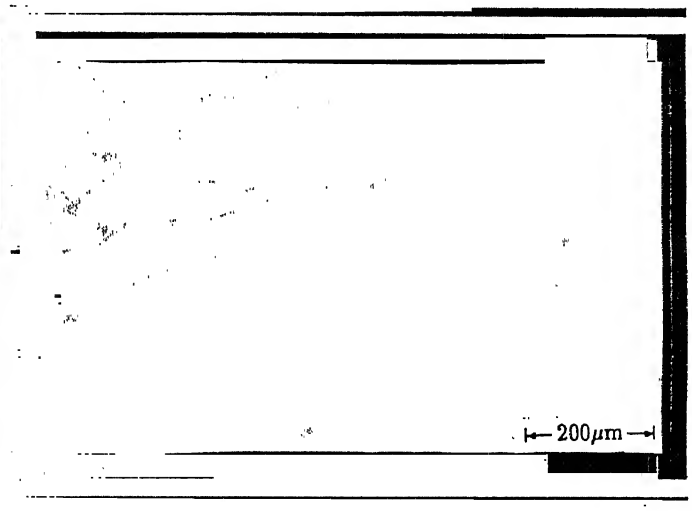

(e).Rolled at 1150 °C

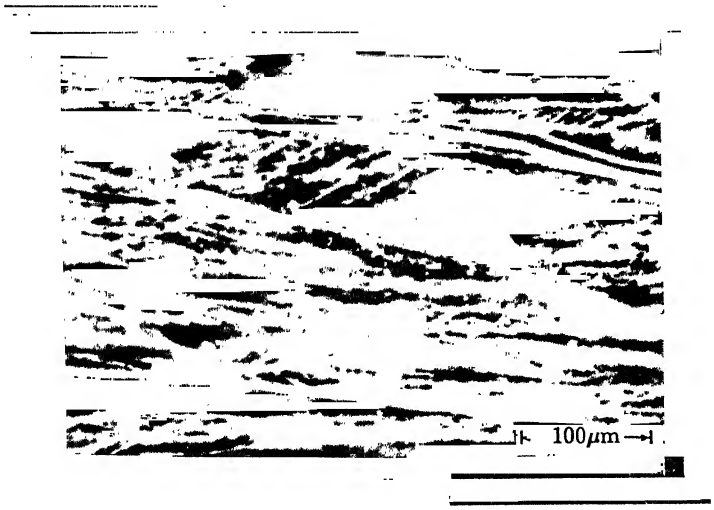

(c). Rolled at 950 °C

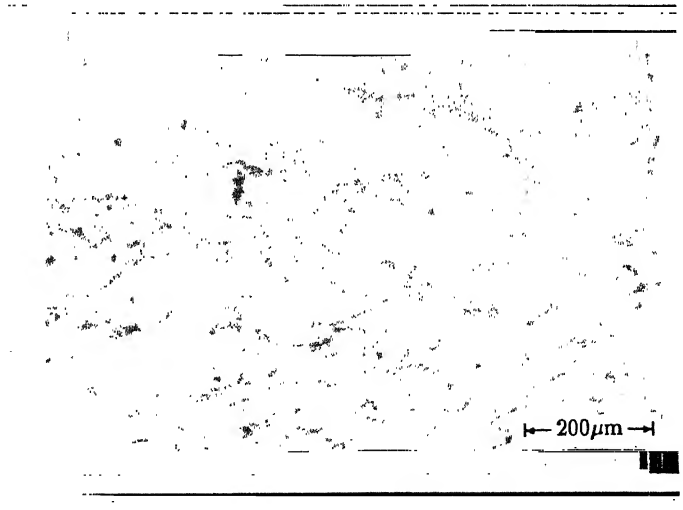

(f).Rolled at 1250 °C

Fig.4.6 Optical micrographs of hot rolled samples after aging at 750 °C for four hours

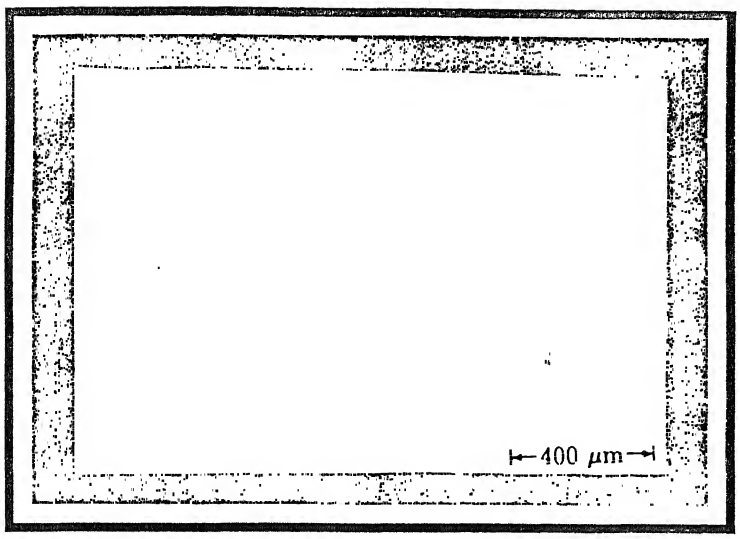

(a). Solutionized sample

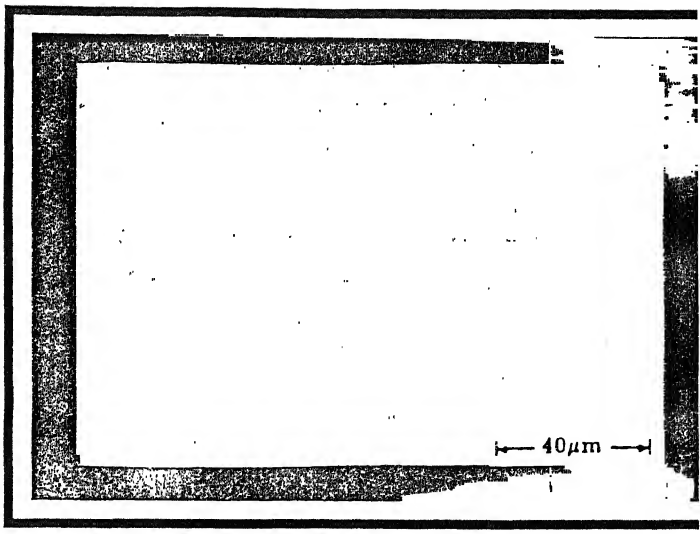

(c). Rolled at 1050 °C

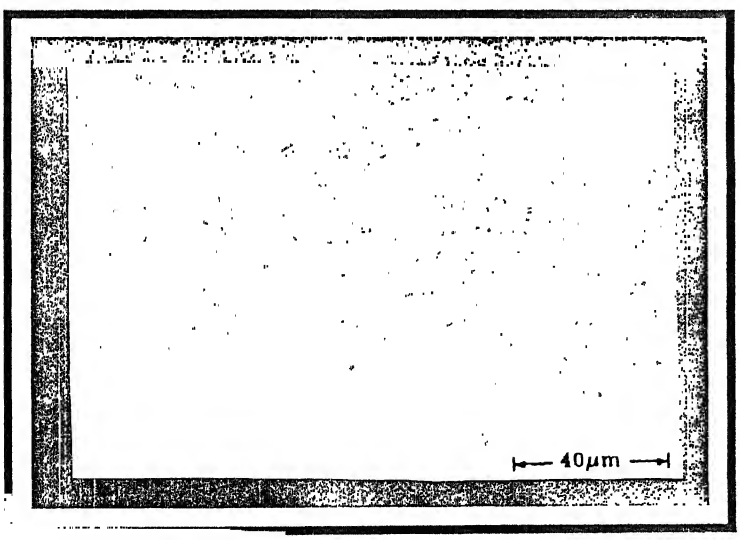

(b). Rolled at 850 °C

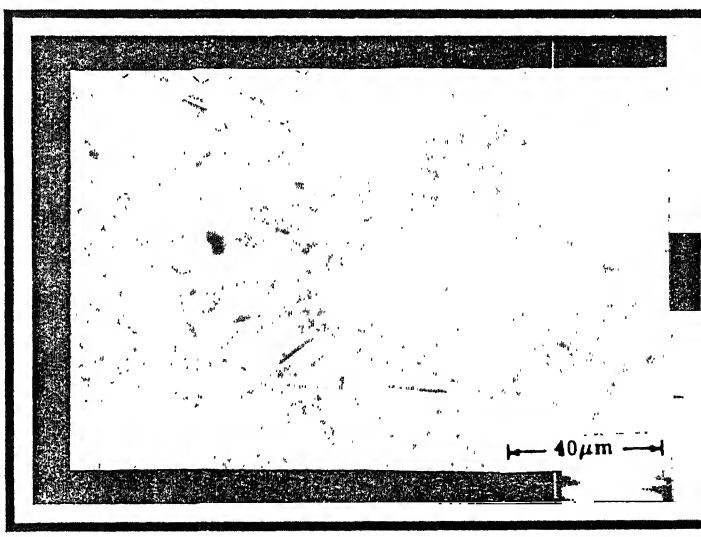

(d).Rolled at 1150 °C

Fig.4.7 .Optical micrographs of the samples after aging at 1050 °C for four hours.

4.3.2 Carbide Analysis

Qualitative analysis of the microstructures has been done with the help of optical microscope and scanning electron microscope. The results obtained are summarized in Table.4.3 . Grain size for all the conditions were measured with optical microscope. whereas precipitation volume fraction, locations, and morphologies were analyzed from SEM micrographs. The obtained results are categorized as follows:

(I) Grain Boundary Precipitates

The continuity of precipitates along the grain boundaries is absent in TMT. Samples for rolling temperature below 1050 °C. For rolling temperature 1150 °C in combination with aging temperatures below 950 °C, a little continuity of precipitates along the grain boundaries reappears. For aging temperature 1050 °C. HT samples shows fine precipitates along the boundaries where as TMT sample has large discrete precipitates on the boundaries.

(II) Matrix Precipitation

Scanning electron microscopy revealed a greater amount of precipitates within the grains in TMT samples (rolled below 1050 °C) Vs HT samples. For aging temperature 950°C all ITMT samples (rolled below 1050 °C) shows homogeneous distribution of fine precipitates over the matrix. This features is shown in Fig. 4.8. Matrix precipitation is absent for aging temperature 1050 °C in all TMT and HT samples.

(III) Precipitates along Shear Bands and Annealing Twins

Samples rolled below 950 °C and aged below 850 °C for 4 hours shows some distinct precipitates along the shear bands. Fig. 4.9 shows that, for higher times of aging shear bands are not well defined. In this case precipitates distribution over the matrix is not homogeneous.

Table 4.3 MICROSTRUCTURAL ANALYSIS

Thermo mechanical Treatment		Grain Size	Carbide Size	Carbide Locations			Carbide Morphology
Solutionizing + Hot Rolling	Aging			Grain Boundary	Matrix	Others	
A. Solutioning at 1250 ^{0}c for 1h 30 min.	No	-	-	-	-	-	No precipitates were identified
AGEING BELOW 950C TEMPERATURE							
A	750 ^{0}c	~0.5-0.6mm	0.25 μm	very few, not continuous	-	-	Spherical
A	850 ^{0}c	~0.5-0.6mm	0.5 μm, sph 1-3 μm, acicular	continuous grain boundary carbide + dense near grain boundary carbide	few of fine precipitates for higher time of ageing	-	spherical, cubical and acicular
B. A+ Hot rolled at 850 ^{0}c	750 ^{0}c	~95 μm with ~1.29 mm length	0.25-0.35 μm	discrete grain boundary carbide	for 1, 4 hours no matrix carbide. for 8, 16 hours within grain boundary where heavily shear bands were present	along the shear bands . for 8, 16 h. shear bands are not well defined	irregular, discrete
-do-	850 ^{0}c	-do-	-do-	-do-	-do-	-do-	-do-
C. A + Hot rolled at 950 ^{0}c	750 ^{0}c	~ 1.1 mm length ~ 65 μm width	-do-	-do-	-do-	-do-	-do-
-do-	850 ^{0}c	-do-	-do-	-do-	-do-	-do-	-do-

(contd.)

Thermo mechanical Treatment		Grain Size	Carbide Size	Carbide Locations			Carbide Morphology
Solutionizing + Hot Rolling	Aging			Grain Boundary	Matrix	Others	
D. A + rolled at 1050 ^{0}c	750 ^{0}c	~ Below 10 μm	0.25-0.75 μm	discrete grain boundary carbide	large bulky carbides homogeneously distributed over the matrix	-	coarse, irregular carbides
-do-	850 ^{0}c	~ 25 μm	-do-	-do-	-do-	-do-	-do-
E. A + rolled at 1150 ^{0}c	750 ^{0}c	- 75-90 μm	0.25 μm	grain boundary carbide are not perfectly continuos	very small fraction of carbides rarely observed	a no. of parallely oriented lines of carbide observed in almost all microstructures; these are also not perfectly continuos	spherical, carbides on the printed lines looks like acicular
-do-	850 ^{0}c	~ 75-90 μm	-do-	-do-	-do-	-do-	-do-
AGEING AT 950C TEMPERATURE							
A	950 ^{0}c	- 0.5-0.6mm	0.15-0.5 μm	continuos grain boundary carbides + dense near grain boundary carbides	-	-	regular spherical

(contd.)

Thermo mechanical Treatment		Grain Size	Carbide Size	Carbide Locations			Carbide Morphology
Solutionizing + Hot Rolling	Aging			Grain Boundary	Matrix	Others	
B. A + rolled at 850 ^{0}c	950 ^{0}c		0.15-0.3 μm	-	fine carbides are homogeneously distributed over the matrix	-	very fine regular spherical rarely bulky particles
D. A + rolled at 1050 ^{0}c	950 ^{0}c	8-30μm	0.1-0.25 μm	-	carbides are homogeneously distributed over the matrix	-	very fine, spherical
E. A + rolled at 1150 ^{0}c	950 ^{0}c	90μm	-	same as observed for treatment 'J'	same as treatment 'J'	-	-
			AGING	ABOVE 950C TEMPERATURE			
A	1050 ^{0}c	~ 0.5-0.6mm	-	not perfectly continuos; no near grain boundary carbides	no matrix carbides	carbides along the twin boundaries	-
B	1050 ^{0}c	for 1-4h. ~ 8 μm for 8-16h ~20-30 μm	1-1.5 μm	discrete, bulky	-	-	regular, bulky
D	1050 ^{0}c	8-30μm	1-2 μm	discrete, bulky grain boundary carbides	-	along the twin edges	regular, large, bulky
E	1050 ^{0}c	~ 30-40μm	0.1-0.25 μm and 1-2 μm	discrete, coarse carbides at grain boundary	very few, fine carbides within matrix	-	regular shape, coarse, bulky, fine carbides are spherical

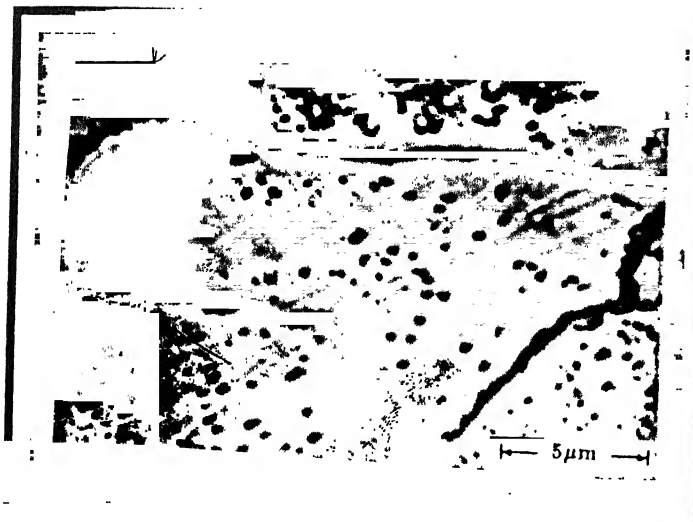

(a). Solutionized sample, aged for 4h.

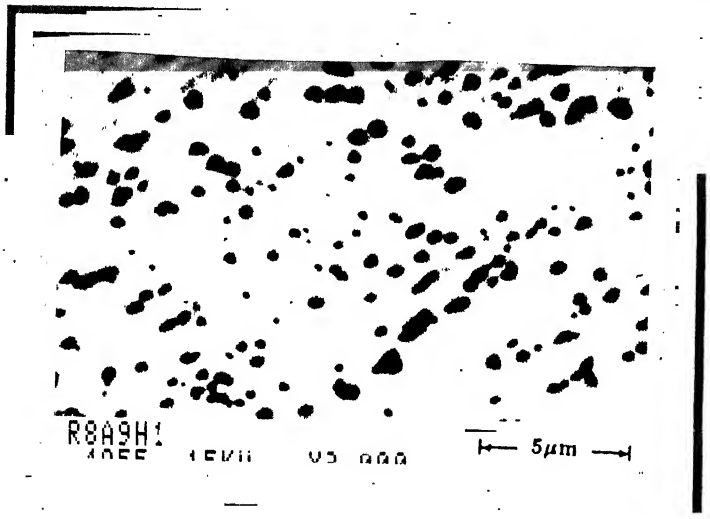

(b). Rolled at 850 °C,& aged for 1h.

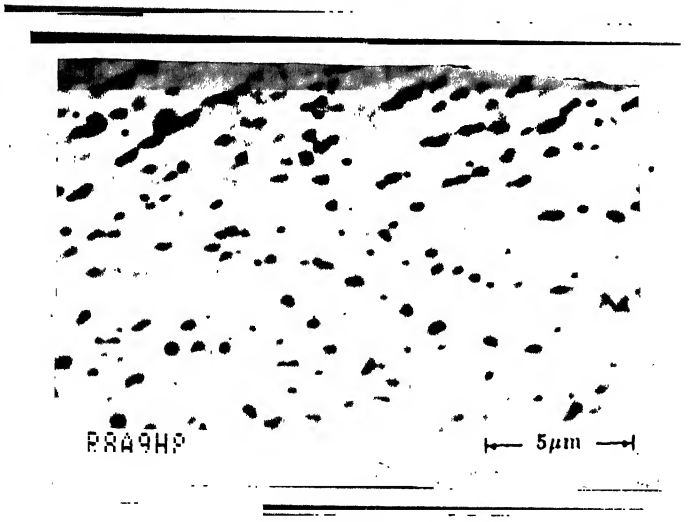

(c).Rolled at 850 °C,& aged for 8h

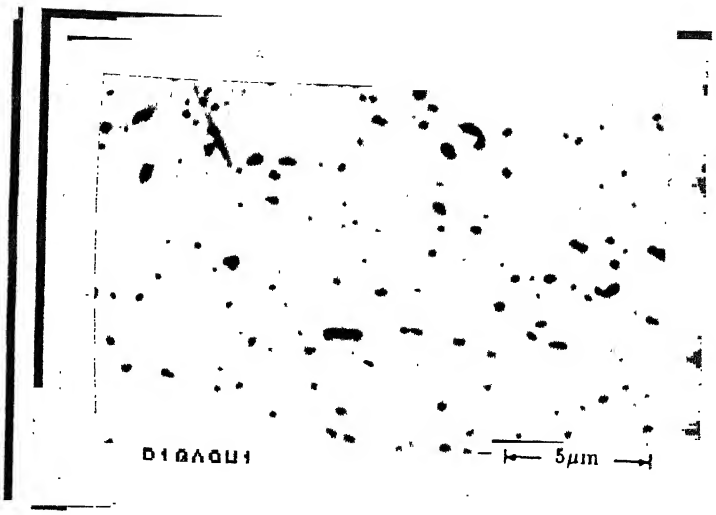

(d). Rolled at 1050 °C, & aged for 1h.

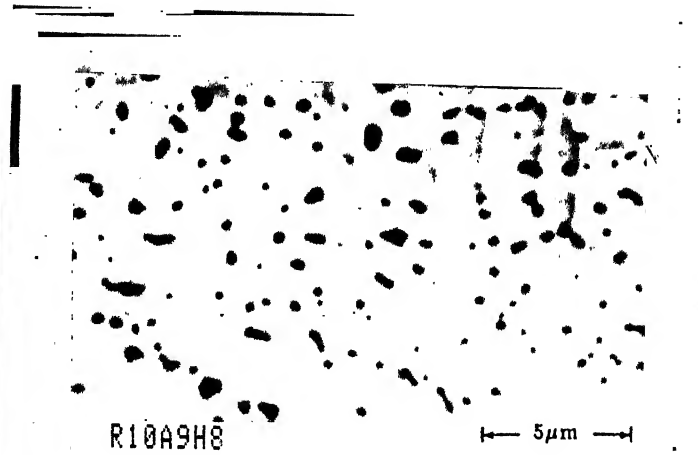

(e). Rolled at 1050 °C,& aged for 8h.

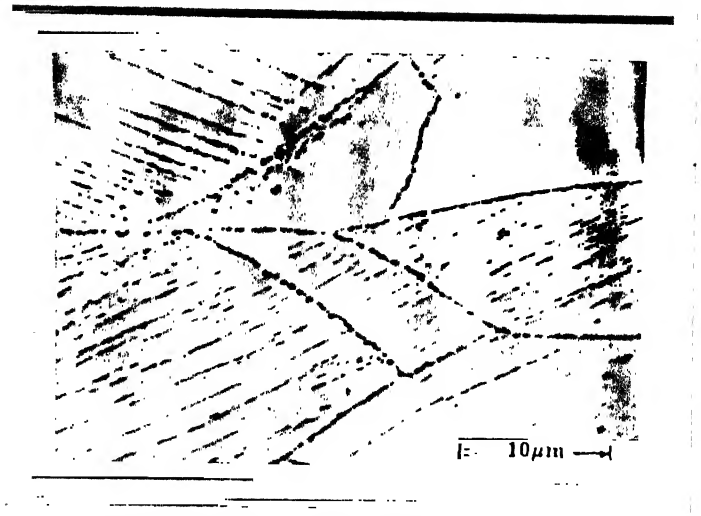

(f).Rolled at 1150 °C,& aged for 8h.

Fig.4.8 .Samples aged at 950 °C , TMT samples shows the fine precipitates homogeneous distributed over the matrix,where as simple heat treated samples shows continuous precipitates along the grain boundaries.

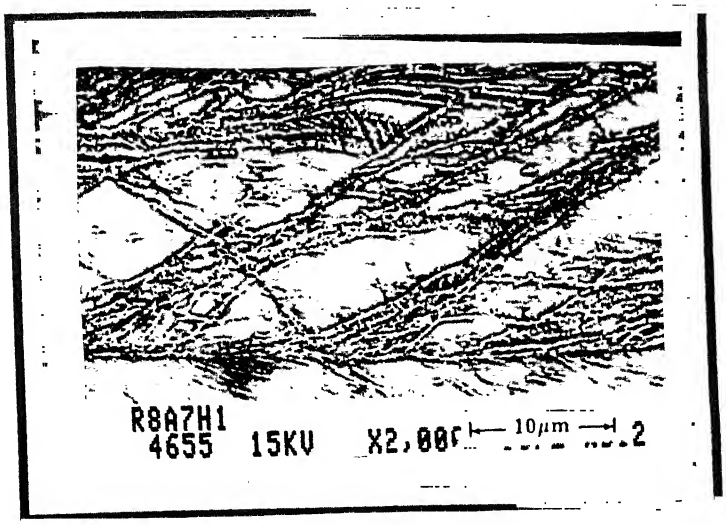

(a).Aged for 1h.

(b).Aged for 1h.

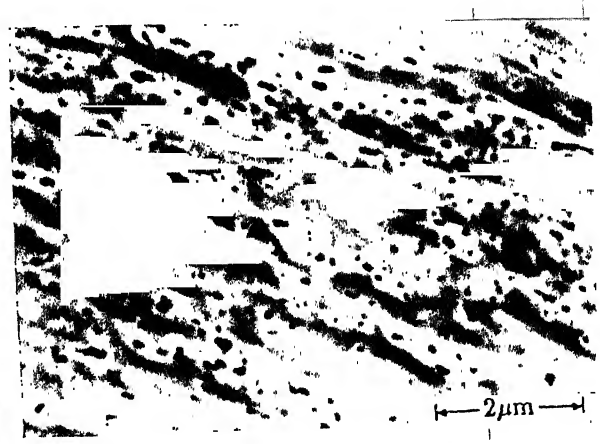

(c). Aged for for 4h.

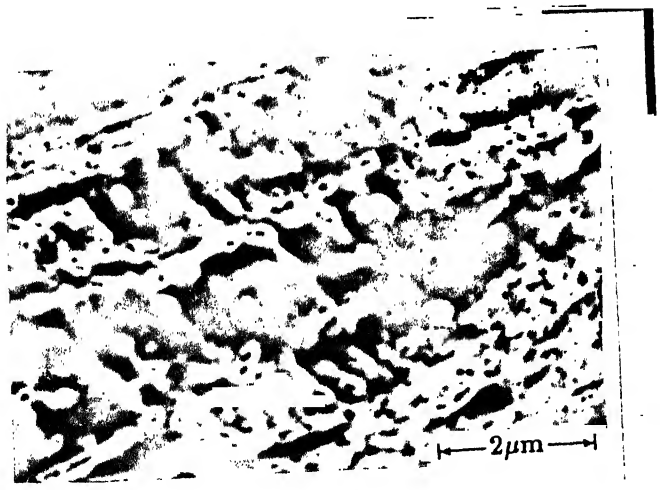

(d).Aged for 8h.

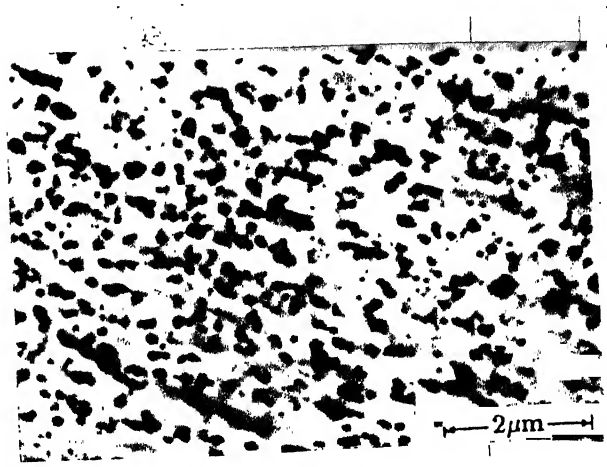

(e).Aged for 16h.

Fig.4.9 .SEM micrographs of the samples rolled at 850 °C showing precipitations along the shear bands after aging at 750 °C

For aging temperature 1050 °C fine precipitates were observed along the annealing twins in HT samples, where as large bulky precipitates were observed at the twin edges in all TMT samples. This is shown in Fig. 4.10(a) to Fig. 4.10(f).

Some oriented lines of precipitates were observed in samples rolled at 1150°C followed by an aging treatment below 950 °C (Fig. 4.8(f)).

From the above results, it is seen that the continuity of precipitates along the grain boundaries are complementary to intense matrix precipitation. If the matrix precipitation increases (in TMT samples), the continuity of grain boundary precipitates decreases, and vice versa (in HT samples).

This can be explained with the help of following facts.

(a) The grain boundary area-to-volume ratio of grains are inversely proportional to the average grain size. The grain size in HT samples are 500 μm, where as in TMT samples after recrystallization grain sizes are just 6 - 90 μm. This increases grain boundary area (GBA) per unit volume 06 - 100 times. But the chromium concentration with in the grains remain same.

(b) In the simplest consideration, deformation provides enhanced chromium diffusion through the creation of dislocation "pipes", as well as other crystal defects such as shear bands which provide energetically favorable sites for interior matrix precipitation.

(c) Further more, since coherent twin boundaries appear to devoid of Carbide precipitation, these interfaces may not have diffusivities much different from the bulk, and therefore do not behave at all like high angle grain boundaries insofar as carbide precipitation are concerned [26].

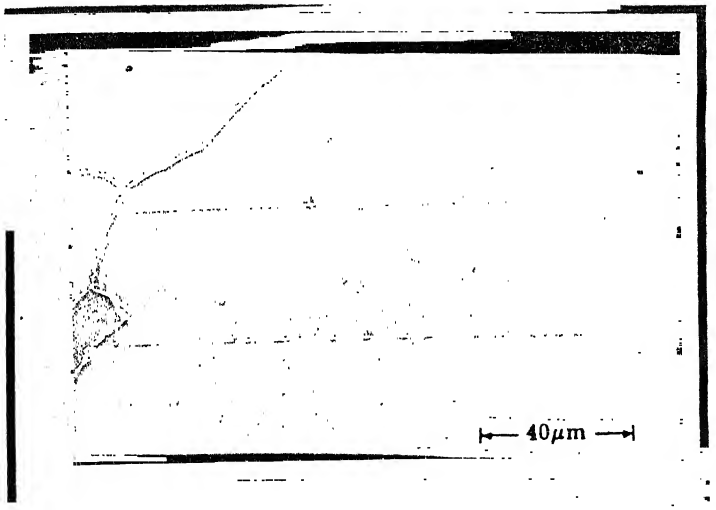

(a). Solutionized sample, aged for 4h.

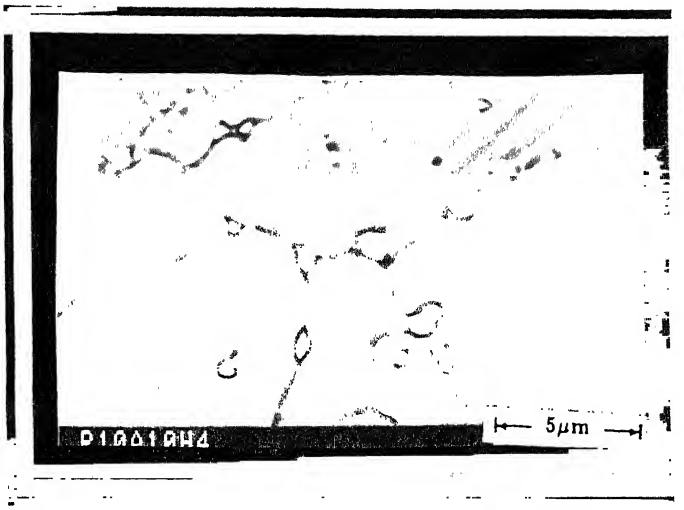

(d). Rolled at 1050 °C, & aged for 4h.

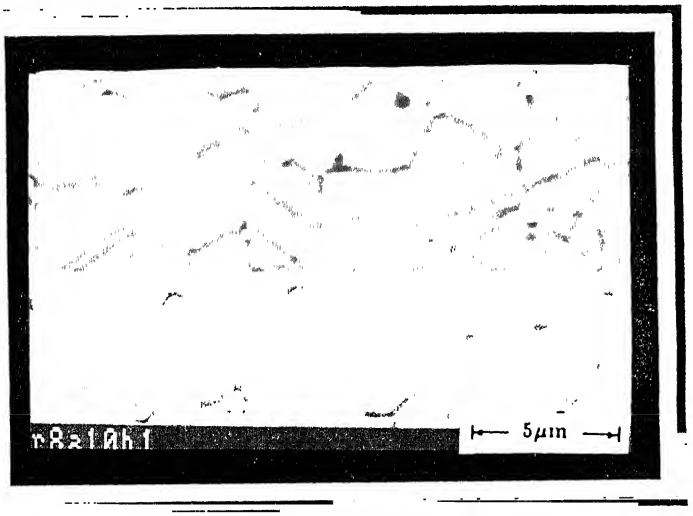

(b). Rolled at 850 °C,& aged for 1h.

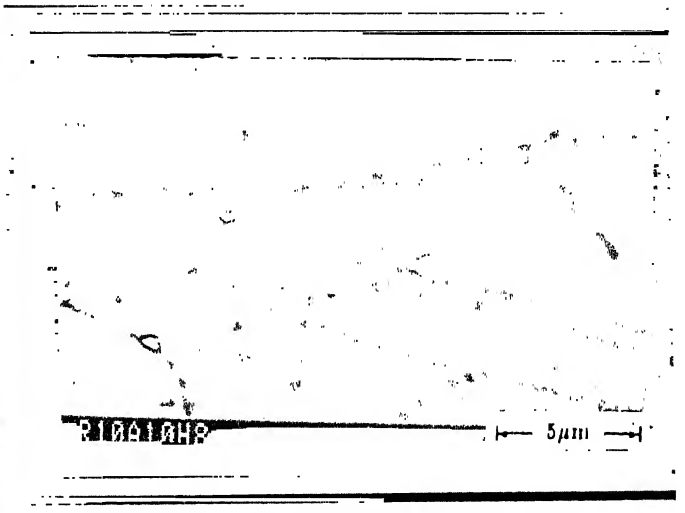

(e). Rolled at 1050 °C,& aged for 8h.

(c).Rolled at 850 °C,& aged for 8h

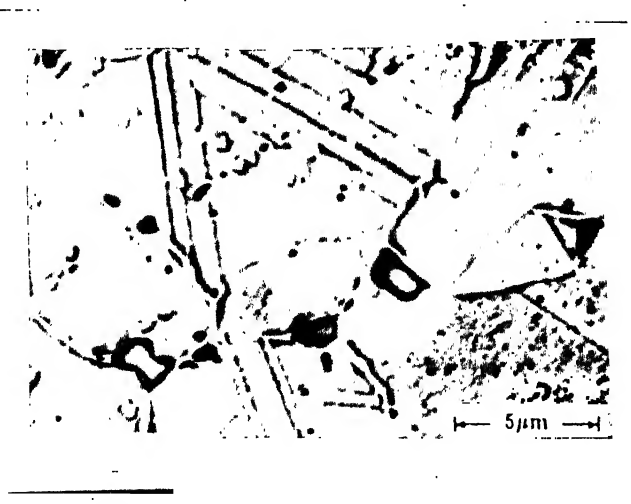

(f).Rolled at 1150 °C,& aged for 4h.

Fig.4.10 .Samples aged at 1050°C , TMT samples shows the discrete and bulky precipitate at the grain edges and annealing twin edges, where as simple heat treated sample shows continuous precipitates along the grain boundaries and twin boundaries.

(d) There should be a critical or minimum chromium concentration to form continuous carbides along the grain boundaries for a particular amount of GBA and deformation induced defect.

Now with the help of above facts we have tried to explain all most all the results. observed from different thermo-mechanical treatment as discussed in next section.

4.3.2.1 Effect of Aging Below 950 °C

For the samples rolled at 850 °C and 950 °C, virtually there is no considerable change in GBA per unit volume, but the amount of deformation induced defects are higher with in the grains. This increases the matrix precipitation. decreasing the grain boundary precipitates. Fig. 4.9 shows the precipitation along the shear bands, with in the grains.

In the case where the samples were rolled at 1050 °C, both recrystallization and deformation effect are present. Although no shear bands observed in rolled samples. but its aspect ratio and hardness measurement indicates that there are some deformation induced defect like dislocation pipes, intersecting. Micro shear bands are present causing the interior matrix precipitation. On the other hand, these samples are being recrystallized below 950 °C, the GBA per unit volume increases 50 ~ 100 times. This decreases the grain boundary carbide continuity.

In the samples rolled at 1150 °C, deformation induced defects are minimum. Fig. 4.4(e) does not shows any shear bendings. and grains are completely recrysgtallized. So there was no matrix precipitation. The grain sizes observed in this case are quite large (70 ~ 90 μm). So the increase in grain boundary area per unit volume is only 6 ~ 9 times. where as in case of working at 1050 °C it increases 50 - 100 time. Most of the carbides observed in this case are along grain boundaries. Since GBA per unit volume increases. it causes a little discontinuity in precipitation along grain boundaries compared to solutionized.

In the HT samples, there is no deformation induced defects. The grain sizes are very large (~ 500 μm). These samples shows the maximum continuity of precipitates along the grain boundary. The dense near grain boundary precipitates shows that, the chromium concentration present in the alloy is much above the critical chromium concentration needed for this grain size. For constant aging time, the precipitates continuity increases with increasing temperature. This is due to increase in diffusivity of chromium with increasing temperature.

For quantitative analysis, volume fraction of precipitates were measured from SEM micrographs using a rectangular grid of 99 points. All the result is shown in Fig. 4.11 to 4.14. For aging at 750 °C, the Figs. 4.11 to 4.14 shows that volume fraction of precipitates in HT samples always smaller than the volume fraction of precipitates obtained from TMT samples for corresponding times. Assuming the volume fraction of precipitates is zero for solutionized condition, we can say that the rate of precipitation is smaller in HT samples than TMT samples, this is because deformation provides enhanced chromium diffusion through the creation of dislocation "pipes", as well as other crystal defects. For the working temperature 1150 °C, there is minimum deformation effect. so again its precipitate volume fraction is comparable to HT samples.

Fig. 4.11 to 4.14 shows that in all cases, as aging temperature increases from 750°C to 950°C, the volume fraction of precipitates increases (This result is exactly opposite in sample worked at 1050°C). This is because, both the solubility of carbon and diffusivity of chromium increases with temperature, however at low temperature both carbon solubility and chromium diffusivity are low enough retarding the precipitation kinetics.

4.3.2.2 Effect of Aging at 1050 °C

Samples aged at 1050 °C behaves quite different from all other cases. In this case the temperature of working has no effect, as for as qualitative behavior of precipitates are concerned.These samples has neither matrix precipitation's nor continuous precipitates

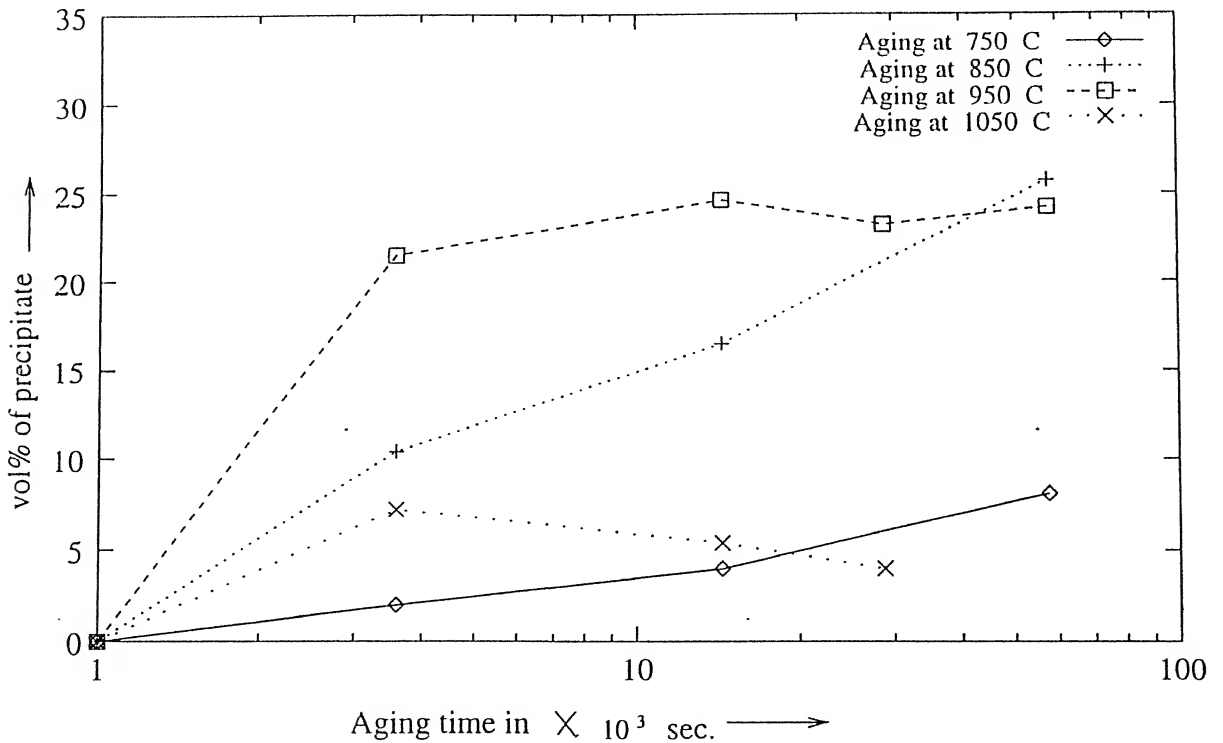

Fig.4.11.Vol% of precipitates vs aging time,in the solutionized

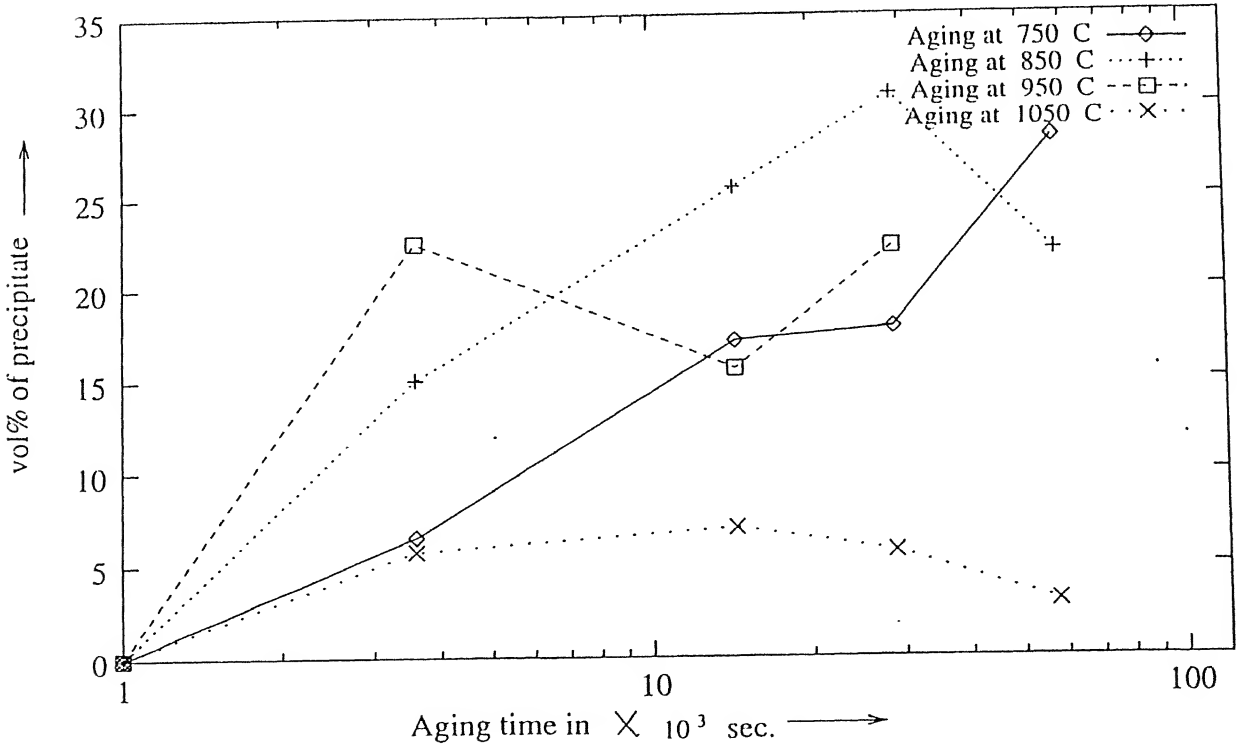

Fig.4.12.Vol% of precipitates vs aging time,in the samples rolled at 850 C

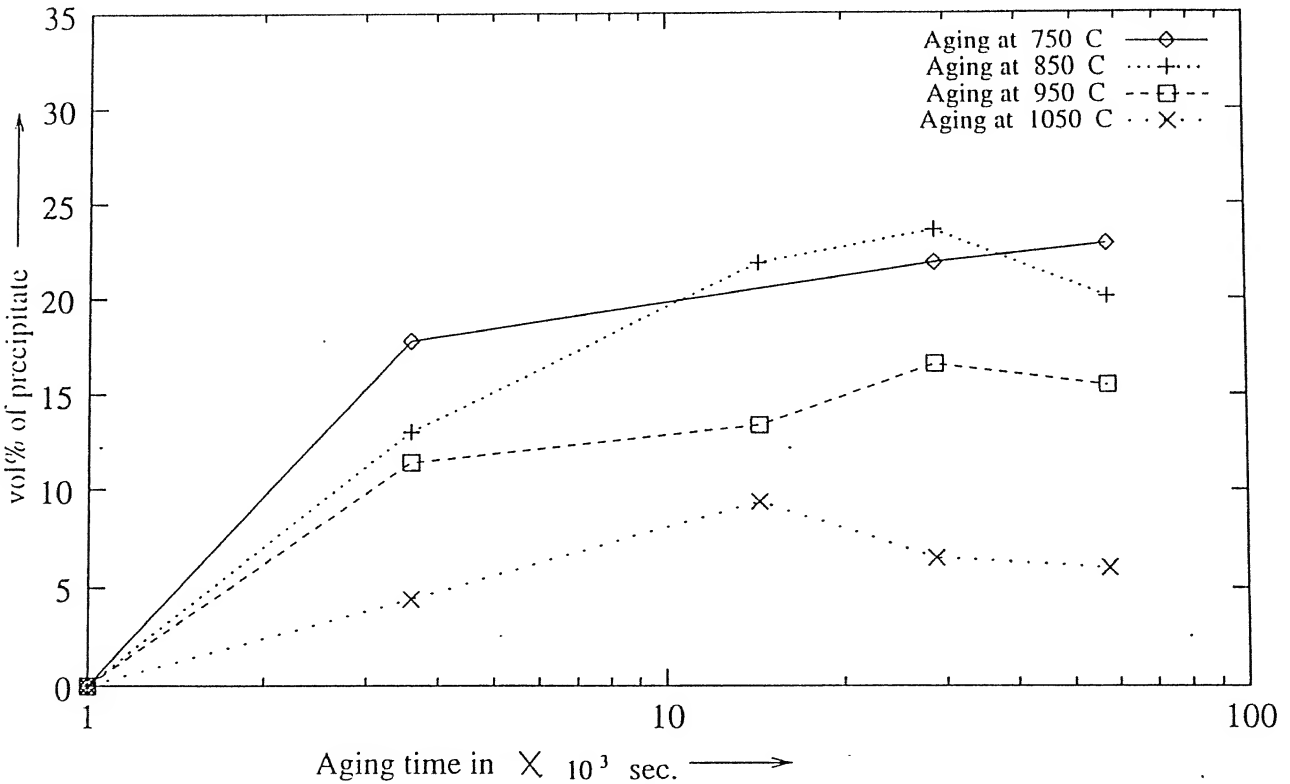

Fig.4.13.Vol% of precipitates vs aging time,in the samples rolled at 1050 C

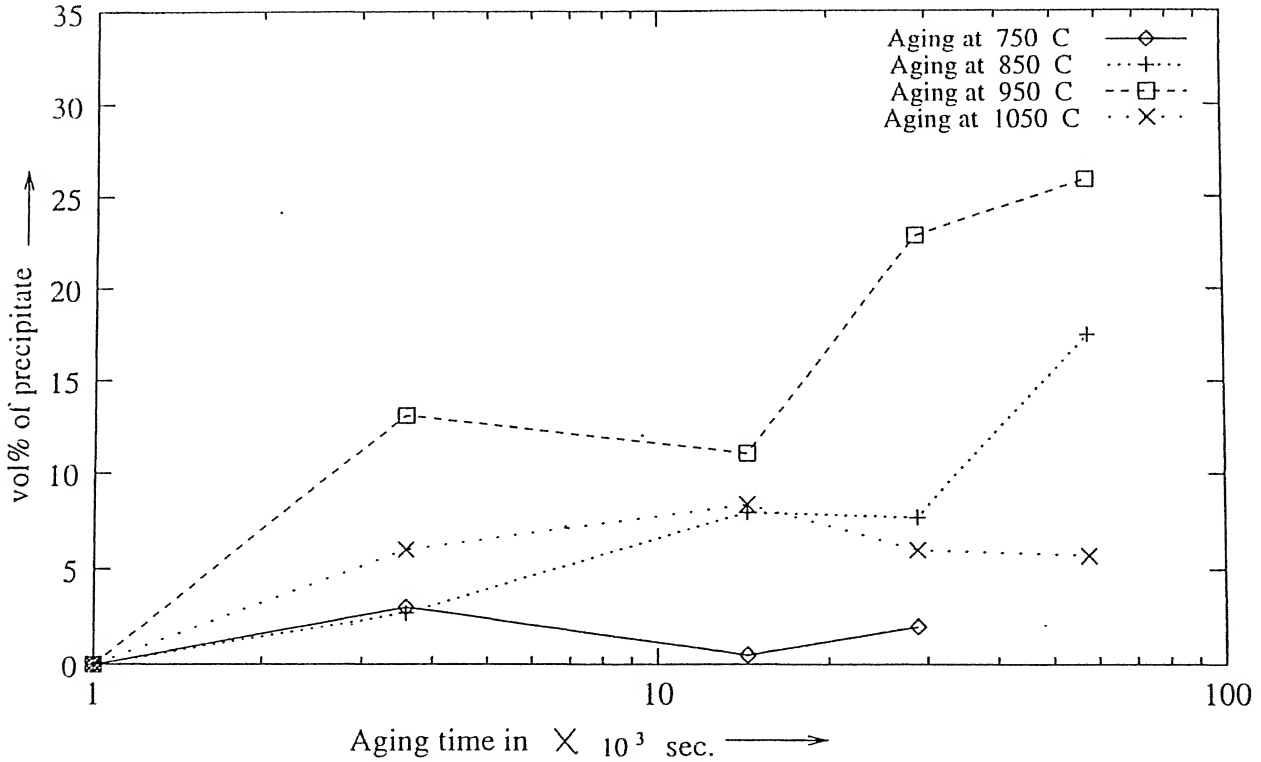

Fig.4.14.Vol% of precipitates vs aging time, in the samples rolled at 1150 C

along the grain boundaries. There are some large bulky discrete precipitates along the grain boundaries and at the twin edges.

In all the TMT samples, at aging temperature 1050 °C, simultaneously three processes could occur (I) Recrystallization process, (ii) recovery annealing process and (iii) precipitation reaction process. Among these processes recovery annealing process must be dominated by recrystallization process, as the microstructures (Fig. 4.7) shows recrystallization and a minimum deformation is necessary to use recrystallization.

Recrystallization process and precipitation reaction process are strongly interactive each other. As early recrystallization process, promotes precipitation reaction but the early precipitation reaction process inhibits the recrystallization process. Since all precipitation were observed only at grain edges and twin edges, one can assume that the recrystallization process was completed much before the precipitation reaction started. This means most of the deformation induced defects were annealed through the recrystallization process and self annealing processes, before the precipitation reaction to occur in the interior of the grains. This causes the lack of matrix precipitation.

These precipitates morphologies and other characteristics are quite similar to that of M_6C carbides as reported in literature [1]. The phase diagram for HS-188 (Fig.1.4) also shows that at 1050 °C, M_6C are more stable precipitates than $M_{23}C_6$ precipitates.

In both the route HT and TMT, the volume fraction of precipitates again come down for aging temperature 1050 °C. This results may be attributed to the following facts (I) at very high temperature, the carbon solubility is increases significantly and even though chromium diffusivity increases, precipitation and precipitate growth ceases, (ii) This temperature may be above the solvus temperature of major carbides $M_{23}C_6$. (iii) As explained in qualitative analysis, the nucleation sites and high diffusivity path within the grains may ceases before the precipitation reaction starts.

4.3.3 Precipitation Kinetics

We have taken an attempt to calculate the activation energy for precipitation formation reaction. We have used precipitation kinetics equations [27].

$$Y = 1 - e^{-kt}$$

where,

Y = Volume fraction of precipitates

k = Reaction constant

$k^{1/n} = K_o\, e^{(-Q/RT)}$

Q = Activation energy for precipitation reaction

T = Temperature

R = Universal gas constant

for small volume fraction, at the beginning of precipitation reaction, the above relationship reduces to

$$Y = [K_o t\, e^{-Q/RT}]^n$$

for constant Y,

$$\log (1/t_c) = \log K_o - Q/RT + \text{const.}$$

In general precipitation kinetics, K_o is constant. So log $(1/t_c)$ vs. 1/T should be a straight line with activation energy as slope.

Fig. 4.15 shows the variation of log (1/t) vs. (1/T), for different working conditions. The activation energy was calculated for solutionized, samples, worked at 850 °C and worked at 1150 °C, are 207 kJ $mole^{-1}$, 53.4 kJ $mole^{-1}$ and 48.8 kJ $mole^{-1}$ respectively. In all the cases the values of Q estimated is lower than that of self diffusion of chromium (307 kJ $mole^{-1}$ for HS 21) [28]. The activation energy of grain boundary diffusion is known to be three quarters or one half of that of self diffusion. Therefore, the value obtained above for solutionized samples (207 kJ/Mole) is considered to be the activation energy of grain boundary diffusion for chromium. However the exact activation energy of grain boundary diffusion for chromium is not available in literature. But the

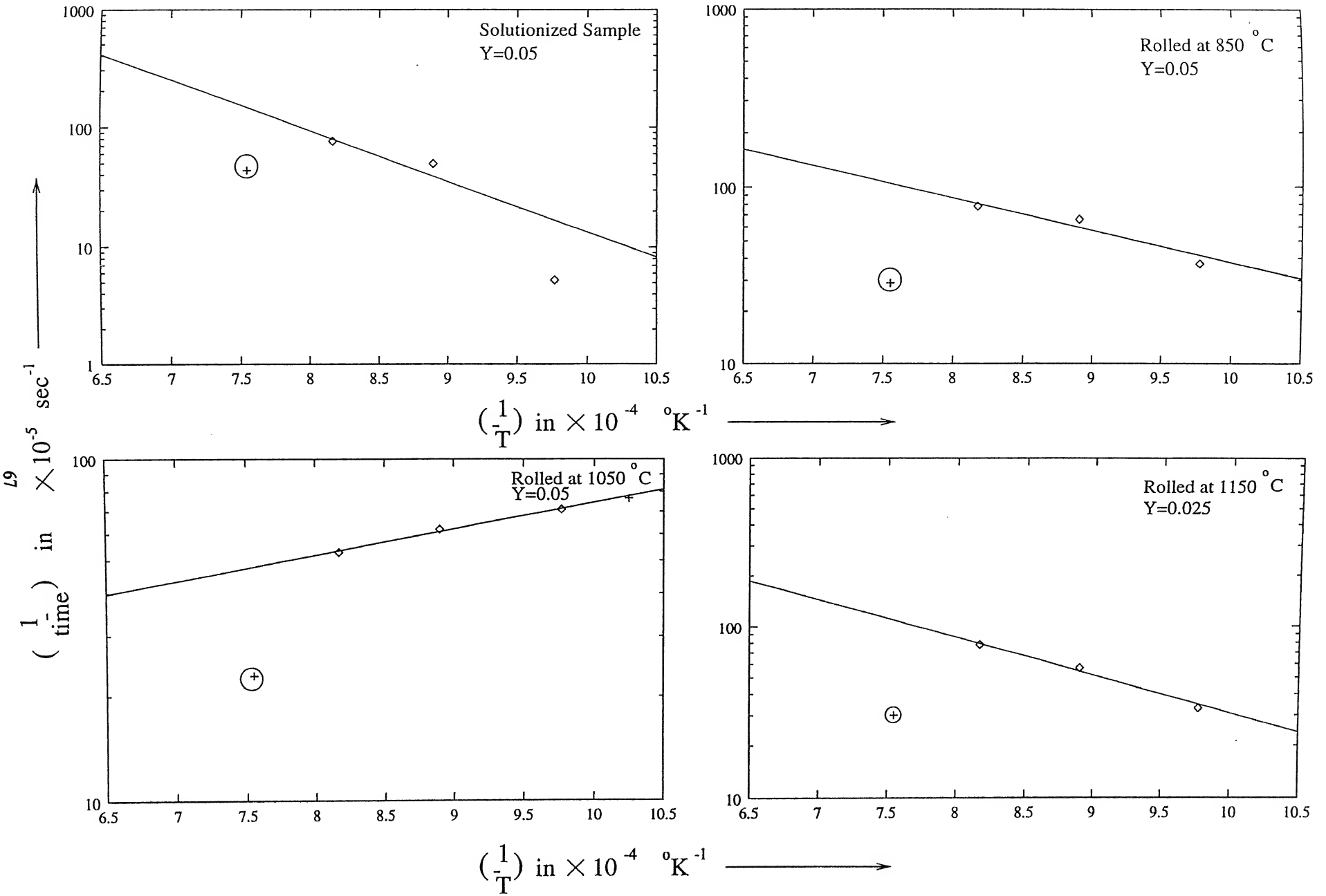

Fig.4.15 .Inverse time-temperature plot for a constant Y(volume fraction)

value we have estimated here was came in the same order as that of reported activation energy of chromium diffusion in other cobalt alloys. The more accurate value of this activation can be obtained by taking more number of observation.

The activation energy obtained for 850 °C is 53.4 kJ/mole and for 1150 °C is 48.8 kJ/mole are very compared to lattice and grain boundary diffusion activation energy. This is because the diffusion processes in these conditions are stress assisted diffusion processes. Stress field around an interstitial atom in a solid solution is such that the atom can be attracted to a dislocation. Thus the precipitation rate on dislocations will be increased owing to stress-induced drift which is superimposed on the drift due to any concentration gradient. Thus more is the deformation induced stress in sample, less is the activation energy required for precipitation reaction.

In fig. 4.15, it is observed that, the data obtained from sample worked at 1050 °C. does not fit to the above relationship. This an unexplained fact, as there is a complex interaction of grain size, deformation, aging temperature, aging time, solubility of carbon and diffusivity chromium on the precipitation kinetics. However, it must be unequivocally stated that because of the scatter and limited range of data in Fig. 4.15, other factors may also contribute to these trends

4.4 EFFECT OF HOT ROLLING TEMPERATURE AND AGING TREATMENT ON THE HARDNESS OF THE ALLOY

Hardness variation of all the samples were tried to measure with "Rockwell C" indentor. All TMT samples has shown Rc values ranging from 20 to 50, but HT samples could not show any Rc values. Hardness of these samples were taken in Rockwell B scale with 100 kg load. These R_B values obtained are in the range of 76 to 88 R_B. Comparing the hardness numbers Rc (150 kg load) with R_B (100 kg load, 1/16 Braille) from the *ASM metals* reference *book*[29], 76-88 R_B is equivalent to 0.3 to 7 Rc values for steels. Using this data we can say that the hardness of HT samples were below 8 Rc.

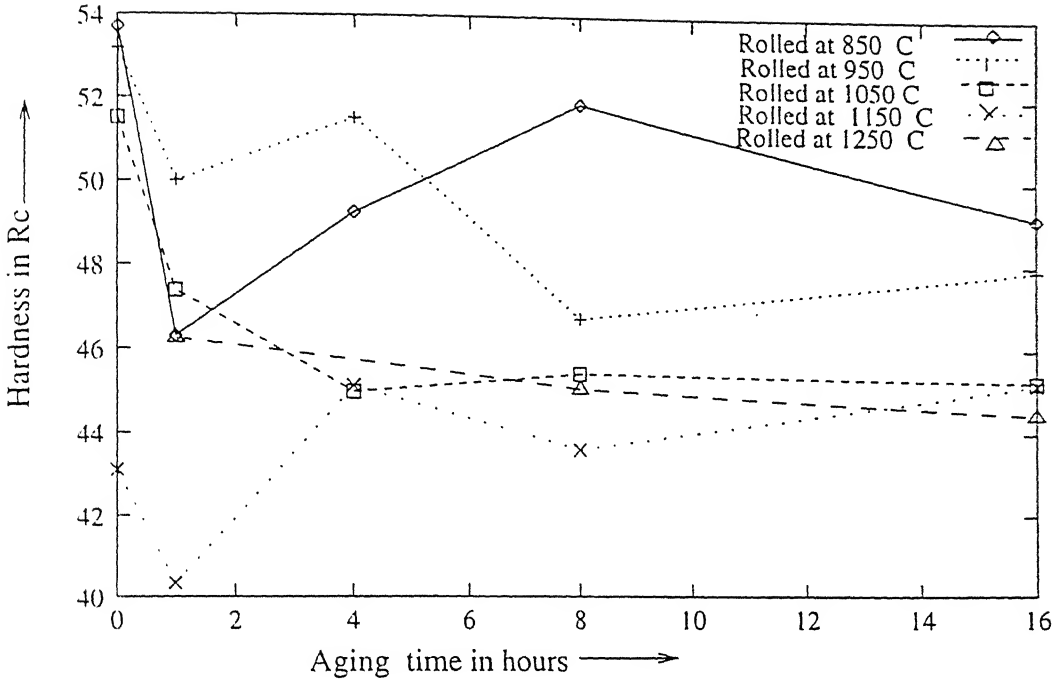

Fig.4.16 .After aging at 750 C,Hardness vs aging time.

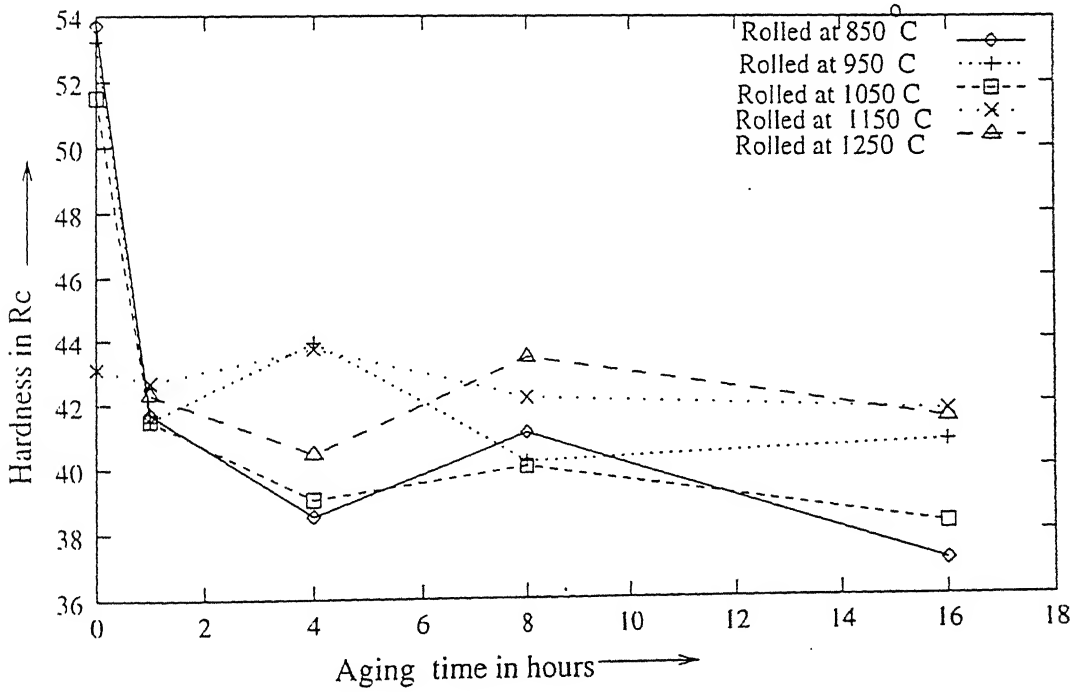

Fig.4.17.After aging at 850 C,Hardness vs aging time.

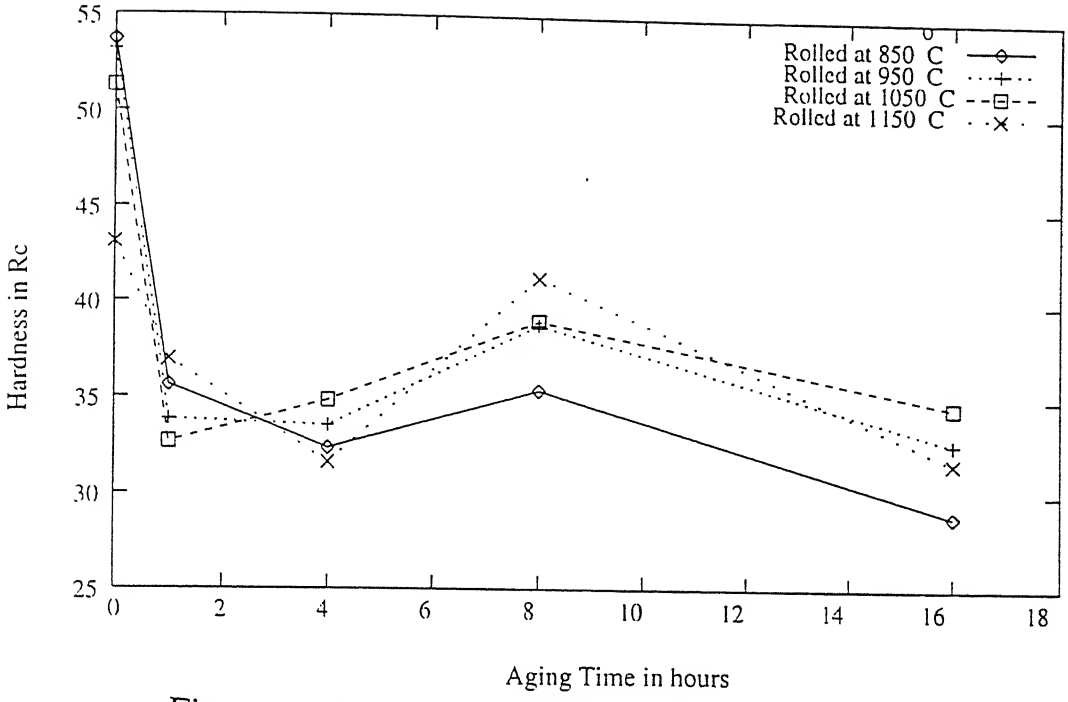

Fig.4.18.After aging at 950 ℃,Hardness vs aging time

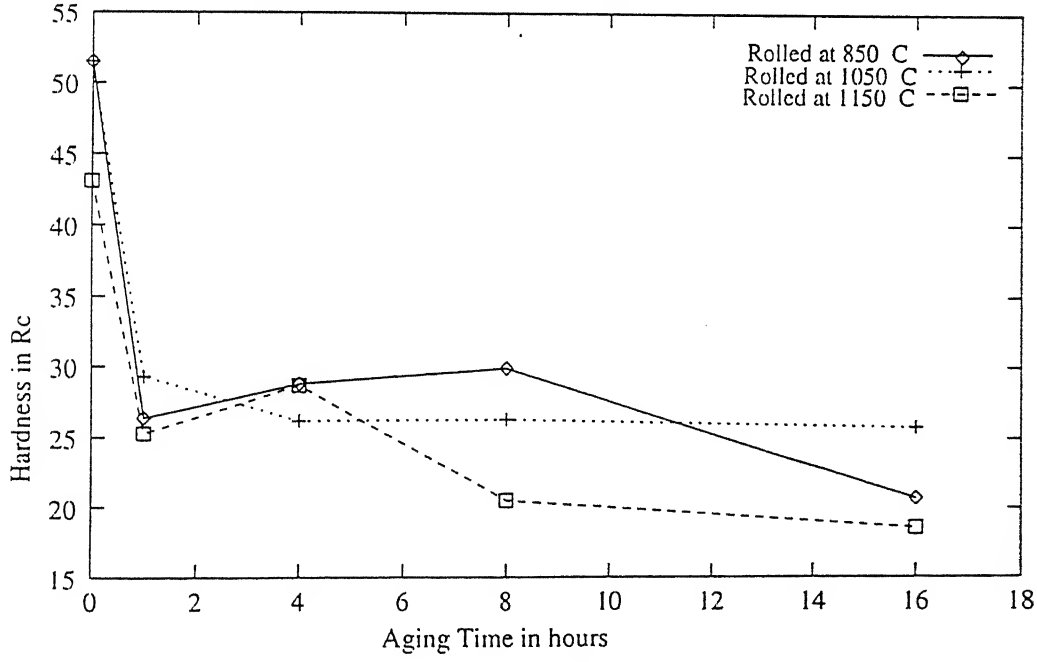

Fig.4.19.After aging at 1050 ℃,Hardness vs aging time

Table 4.4 shows the variation hardness in TMT Vs. HT samples from this data it is observed that the hardness of HT samples are low enough compared to TMT samples. This low hardness may be attributed to the facts (I) HT sample has very large grain size compared to TMT samples, so hardness decreases following Hall-pitch relationship (ii) due to negligible volume fraction of interior matrix precipitation, matrix hardness decreases and (iii) continues carbides along the grain boundaries become the fracture initiation sites in these samples.

Table 4.4 Effect hot rolling and subsequent aging on hardness of superco-605

Aging Temp. (in °C)	Thermo-mechanically treated		Heat Treated	
	Hardness Rc	Vol. % pptn	hardness R_B	Vol. % pptn
750	40 - 51	2 - 28	78 - 84	2 - 8
850	37 - 44	2.7 - 25	76 - 83	10 - 25
950	31 - 41	11 - 25	82 - 88	21 - 24
1050	20 - 30	4 - 9	84 - 86	4 - 7

From the Fig. 4.16 to 4.19, it is observed that, for constant aging time and temperature, the variation of hardness with deformation temperature is very small. This variation is not in systematic. Experimentally observed hardness data points were more scattered in lower aging temperature then in higher aging temperature. It is simply because of the residual stress of working was relaxed during aging. The stress relaxation processes were more active as the aging temperature increases. In table 4.4 it was shown that hardness decreases very fast with increasing aging temperature in TMT sample. Table 4.4 also shows the variation of hardness Vs. precipitation volume fraction. As for as thermo-mechanical processing concerned, effect of precipitation volume fraction on hardness was very less.

CHAPTER 5
SUMMERY AND CONCLUSION

In the present study, the effect of thermomechanical processing on grain boundary reaction as well as on matrix precipitation in the interior of the grains were investigated using a wrought cobalt base superalloy, Superco-605.The aging characteristics of solutionized as well as hot rolled samples were investigated using optical and scanning electron microscope.The conclusions of present study are summarized as follows:

1. SEM revealed a greater continuity of precipitates along the grain boundaries in the undefformed samples Vs deformed samples.
2. The extent of matrix precipitation that occurred during aging also influenced by the temperature of hot rolling. Since the maximum amount of precipitates obtained in both the case were same, hence it is concluded that the interior matrix precipitation were formed in hot rolled samples were in the expense of grain boundary precipitates
3. Solutionized samples did not shows considerable grain growth during aging at the 750°C-1050°C for 1 hour to 16 hours. But hot rolled samples had shown a noticeable grain growth at aging temperature 1050°C for 1 hour to 16 hours. Below 1050°C these samples also did not show any considerable grain growth during aging.
4. At aging temperature below 950°C matrix precipitates were found inhomogeneously distributed over the matrix in the hot rolled samples and at 950°C temperature of aging matrix precipitates were found homogeneously over the matrix. Where as at aging temperature above 950°C no matrix precipitates were observed.
5. The activation energy of precipitation formation reaction was estimated as 207 kj/mole for the early stage of grain boundary precipitation reaction in undefformed sample, and was considered to be the activation energy of grain boundary diffusion of chromium. Activation energy of precipitation formation reaction for the samples deformed at 850°C and 1150°C was

also calculated 53.4 kj/mole and 48.8 kj/mole respectively. This low activation energy is attributed to the stress assisted diffusion of chromium through dislocation 'pipes'.

6. Rockwell hardness of all deformed samples were measured after aging and was produced a systematic decrease in hardness with increasing aging temperature. But no systematic relationship was observed between the hardness and working temperature of thermomechanically processed sample. After aging, the hardness of solutionized samples was observed as below 8 Rc which is well below the hardness observed in thermomechally processed samples.

References

1. C. T. Sims, Superalloys genesis and character *in Superalloys II*, Eds. C. T. Sims,N. S. Stoloff and W. C. Hagel, John wiley & sons,Newyork, 1987.
2. J. R. Stefens, Resources, Supply and Avilability *in Superalloys Supercomposites and Superceramics,* Eds. J. K. Tien and T. Caulfield, Academic press Inc, San Diego,1989, p13.
3. W. Boesch, *in Superalloys Supercomposites and Superceramics,* Eds. J. K. Tien and T. Caulfield, Academic press Inc, San Diego,1989, p3.
4. N. S. Stoloff, Wrought and P/M Superalloys *in Metals hand book*, Eds. ASM International, Materials park 0H, 10th edition, 1990, p950
5. Walter Betteridge, Iron Nickel and Cobalt based superalloys heat resistant alloys *in Material Science and Technology*,Eds. R.M.Cahn, P.Hassan, E.J.Kramer, VCH Publisher Inc., Newyork, 1992, p686
6. F. Schubert, Temperature and Time dependent Transformation: Application to high temperature alloys *in superalloys handbook*, Eds.Mathew J. Donachis Jr., American society for metals, metal park Ohio, 1984, p.71-101
7. Heat treater's guide: Non ferrous alloys, Eds.ASM International, Materials Park OH, 1997,p
8. I. Hiroshi and T. Manabu, Effect of heat treatment on precipitation behavior and high temperature strength in a wrought Co-base superalloy, *J. of Mat. Sci.*, 21, 1986, p2803-2811.
9. J. W. Weeton and R. A. Sighorelli, *Trans. ASM*, 47, 1955, p815.
10. K. Rajan, *Mettal. Trans.*, 13A, 1982, p1161.
11. J. D. Mathew, *Superalloys Source Book* Eds. J. D. Mathew, ASM International , Ohio, 1984, p4.
12. J. D. Mathew, Relation of properties to microstructure *in Superalloys Source Book* Eds. J. D. Mathew, ASM International , Ohio, 1984,
13. W. Betteridge and A. W. Franklin, Effect of heat treatment and structure on the creep and stress rupture properties of Nimonic 80A, *J. Inst. Met.*, 85, 1956-57, p473-479.

14. P.Viatour, J.M.Drapier,D.coutsordis and L.Habraken,:Structure and properties of CM-7 a wrought precipitation -hardening cobalt-base alloy, *Cobalt*, 51, june-1971,p67

15. C.S. Barrettt and T. B. Massalski, *Structure of metals,* Eds. Pergomon press, 3rd edition,1980

16. R.N.J.Taylor and R.B.Waterhouse,: A Study of the aging behaviour of a cobalt based implant alloy, *J of mat .sci.*,18,1983,p3265-80

17. *Atlas of creep and stress rupture curves*,Eds. Howard E. Boyer, ASM International, metal park ohio 1988,p

18. C.T.Sims,: Cobalt-base superalloys *in Superalloys*, Eds.John wiley and sons,New york,1972,p161-162.

19. R.L.Fleicher,Acta met.,11,(1963),p203

20. H.W.King,:Alloying behaviour and effect in concentrated solidsolution, Eds. T.B.Massalski, Gordon & Breach, Newyork 1965,p65

21. Manabu Tamura, Alloying effect on hot defformation *in Superalloys Supercomposites and Superceramics,* Eds. J. K. Tien and T. Caulfield, Academic press Inc, San Diego,1989, p220.

22. J. L. De Mol Van Otterloo and M. de hosson, Microstructural features and mechanical properties of a Cobalt based laser coating , *Acta Mat.* Vol 45, No.3, 1997, p1225-1236

23. L.A.Pugliese and J.P.Stroup,: A New Co-Ni-Mo-Cr ultrahigh-strength corrosion-resistant alloy system:multiphase,*Cobalt*,43,June-1969,p80-86

24. A.B.Lerch and V.Gerold, *Met. trans.*, 18A,1987,p2135-2141

25. A.B.Lerch, N.Jayanarayan and S.D.Antolovich, *Mat.Sci. and Engg.*, 66,1984, p151-166

26. A. E. Trillo, R. Beltran, J. G. Maldonado, R. J. Romero, L. E. Murr,W. W. Fisher and A. H. Advani, *Materials Characterization*, 35, 1995, p99.

27. A. K. Jena, *Phase transformation in materials,* Prentice Hall, Engle wood cliffs,New Jersy, 1992, p342.

28. R. Hashiguchi and T. Chikazumi, *Crystal lattice deffects*, Eds. Asakura, Tokyo, 1990, p181.

29. *ASM Metals Reference book*, Eds. Michael Bauccio, ASM International, The Materials Information Society, Materials park OH, 1993, p223-228